THE ASTROPHYSICAL JOURNAL, 558:780–801, 2001 September 10

ON THE DYNAMIC STABILITY OF COOL SUPERGIANT ATMOSPHERES

A. LOBEL
Harvard-Smithsonian Center for Astrophysics, 60 Garden Street, Cambridge MA 02138; alobel@cfa.harvard.edu
Received 2001 March 7; accepted 2001 May 7

ABSTRACT

We have developed a new formalism to compute the thermodynamic coefficient Γ_1 in the theory of stellar and atmospheric stability. We generalize the classical derivation of the first adiabatic index, which is based on the assumption of thermal ionization and equilibrium between gas and radiation temperature, toward an expression that incorporates photoionization due to radiation with a temperature $T_{\rm rad}$ different from the local kinetic gas temperature. Our formalism considers the important non-LTE conditions in the extended atmospheres of supergiant stars. An application to the Kurucz grid of cool supergiant atmospheres demonstrates that models with $T_{\rm rad} \simeq T_{\rm eff}$ between 6500 and 7500 K become most unstable against dynamic perturbations, according to Ledoux' stability integral $\langle \Gamma_1 \rangle$. This results from Γ_1 and $\langle \Gamma_1 \rangle$ acquiring very low values, below 4/3, throughout the entire stellar atmosphere, which causes very high gas compression ratios around these effective temperatures. Based on detailed non-LTE calculations, we discuss atmospheric instability of pulsating massive yellow supergiants, such as the hypergiant ρ Cas (Ia^+), which exist in the extension of the Cepheid instability strip, near the Eddington luminosity limit.

Subject headings: instabilities — hydrodynamics — stars: atmospheres — stars: variables: other — supergiants

1. INTRODUCTION

The atmospheres of cool massive supergiants are unstable, which causes pulsation variability, strongly developed large-scale atmospheric motion fields, excessive mass loss, and extended circumstellar envelopes. One of the best studied examples of these very luminous supergiants is the yellow hypergiant ρ Cas (F2-G Ia^+). This evolved star exhibits stable pulsation (quasi) periods of $300-500$ days.

Although the κ- and γ-mechanisms have been identified as the main cause for driving pulsations of the less luminous high-gravity atmospheres of Cepheids, little is known about the efficiency of these effects for the much more extended and tenuous atmospheres of cool massive supergiants. In detailed calculations of the first generalized adiabatic index Γ_1, Lobel et al. (1992; Paper I) found that this quantity assumes very small values, below 4/3, in low-gravity model atmospheres with $5000 \leq T_{\rm eff} \leq 8000$ K, primarily because of the partial thermal ionization of hydrogen. Stothers & Chin (1999) recently suggested that enhanced mass loss due to ionization-induced dynamical instability of the outer envelope of luminous supergiants that evolve redward would terminate their redward movement, and provide an explanation for an observational lack of yellow and red supergiants with $\log (L_*/L_\odot) \geq 6.0$.

However, the major problem for evaluating supergiant dynamic (in)stability, based on detailed calculations of Γ_1, is the breakdown of LTE conditions in these very extended atmospheres. The importance of non-LTE (NLTE) ionization and excitation conditions is evident from modeling the spectra of these stars, which are formed in conditions of very small gravity acceleration. The local ionization equilibrium is strongly determined by the stellar radiation field, which determines important thermodynamic quantities such as the heat capacities and the related mechanic compressibility of these atmospheres.

In this paper we develop, for the first time, a self-consistent thermodynamic formalism which accounts for departures from LTE for the calculation of Γ_1. This goal is accomplished by introducing the temperature of the radiation field as an independent state variable, which can differ from the local kinetic gas temperature. We discuss in § 2 the departure from thermal ionization equilibrium by an incident and diluted stellar radiation field in the Eddington approximation. Section 3 provides a historical overview of the development of the theory of the adiabatic indices. The complete analytical expressions for the computation of Γ_1 and the heat capacities in mixtures of monatomic gas interacting with radiation are given in § 4. We account for departures from LTE conditions due to the interaction of matter and radiation by evaluating the thermodynamic quantities accordingly. Section 5 presents a discussion of the effects of NLTE conditions on Γ_1 in cool supergiants. These detailed NLTE calculations of Γ_1 are applied in § 7, to evaluate their dynamic stability according Ledoux' stability integral $\langle \Gamma_1 \rangle$ for radial fundamental-mode oscillations (§ 6). We apply our calculations to a new (Kurucz) grid of cool supergiant model atmospheres, which we compute down into the stellar envelope. We demonstrate that NLTE ionization of hydrogen strongly enhances the destabilization of supergiant atmospheres with $6500 \leq T_{\rm eff} \leq 7500$ K. For models toward smaller gravity acceleration the stability integral decreases, and the destabilizing regions occur at lower densities over a larger geometric fraction of the atmosphere. A discussion of these results in relation to pulsation driving in yellow hypergiants, and in atmospheric instability regions recently identified in the upper portion of the H-R diagram by de Jager & Nieuwenhuijzen (1997), is given in § 8. The conclusions of this theory and application are listed in § 9.

2. NON-LTE IONIZATION

In the atmospheres of supergiants the ionization balance of tenuous gas is not solely determined by a collisional equilibrium according to the Saha equation. Significant departures from thermal (equilibrium) ionization occur due to photoionization by an incident radiation field. The local ionization state then becomes dependent on both kinetic

gas temperature and the temperature of the radiation field. For example, stellar UV radiation strongly influences the Balmer continuum in hot stars. In deeper atmospheric layers, where the atmosphere is sufficiently optically thick for all wavelengths, both temperatures thermalize, and the equilibrium radiation field assumes an intensity distribution determined by the local kinetic gas temperature. In the upper layers the radiation field dilutes with distance from a point in the atmosphere where the gas becomes sufficiently optically thin, and the radiation temperature decouples from the local thermodynamic conditions.

2.1. *Eddington Approximation*

A comprehensive description of partially ionized systems that deviate from equilibrium because of a radiation field of temperature $T_{\rm rad}$, not in equilibrium with the electron Maxwell distribution of temperature T_e, is given in Elwert (1952). All particle components (neutrals, ions, and electrons) are assumed to be in a Maxwell distribution. For the calculation of ionization fractions, this statistical theory assumes that the detailed balance between collisional and/or radiative ionization and recombination processes applies. It enables us to express the ionization fractions through a departure coefficient b from the Saha equilibrium (also the "NLTE Saha equation"), which can be evaluated using a reduced form of the collision ionization cross section and, for the photoionization coefficient, a diluted Planck distribution with a cross section obtained from quantum mechanical calculations. The Elwert equation is given by

$$\frac{n_{j+1}\, n_e}{n_j} = \left(\frac{n_{j+1}\, n_e}{n_j}\right)_{\rm Saha} \frac{1}{b_j}\,, \tag{1}$$

where n_j denotes the number density of particles in the jth ionization stage, and n_e is the electron number density. The Saha-Boltzmann equation for thermal ionization form the rth excitation level is

$$\left(\frac{n_{j+1}\, n_e}{n_j}\right)_{\rm Saha} = 2\,\frac{u_{j+1}}{u_j}\,\frac{g_{r,j+1}}{g_{r,j}}\left(\frac{2\pi m_e\, kT_e}{h^2}\right)^{3/2} \times \exp\left(-\frac{I_j - \chi_{r,j}}{kT_e}\right), \tag{2}$$

with the partition function $u_j = \sum_{r=0}^{\infty} g_{r,j} \exp\,(-\chi_{r,j}/kT_e)$, and where I_j is the ionization energy from the ground state, $\chi_{r,j}$ is the excitation energy of level r, and $g_{r,j}$ its statistical weight. Here h is the Planck constant and the other symbols have their usual meaning. The departure coefficient (for ionization from the ground level) in equation (1) is

$$b_j = \frac{1 + (B/An_e) y_e^{-1/2}\, F(y_e,\, y_e)}{1 + W(B/An_e)(y_e^{1/2}/y_{\rm rad}) \exp\,(y_e - y_{\rm rad}) F(y_e,\, y_{\rm rad})}\,, \tag{3}$$

with the function

$$F(y_e,\, y_{\rm rad}) \simeq \frac{(1 - 1/y_{\rm rad})}{(1 - 2/y_e)}\,, \tag{4}$$

where we denote $y_e = I_j/(kT_e)$ and $y_{\rm rad} = I_j/(kT_{\rm rad})$. Here A and B are constants that depend on the ionization energy, the Thompson cross section, and the Bohr radius. Note that equation (2) depends only on the kinetic gas temperature T_e, whereas equation (1) is dependent on $T_{\rm rad}$ as well. The dilution factor with geometric height d from the stellar surface R_* is

$$W(z) = \frac{1}{2}\left(1 - \sqrt{1 - \frac{1}{z^2}}\right), \tag{5}$$

where $z = d/R_*$. At the surface $z = 1$, the dilution factor $W(z = 1) = \frac{1}{2}$, because a gas particle is irradiated at most by half the stellar hemisphere.

Ecker (1978) distinguished two important conditions of partial ionization from the general equation (1), based on a critical electron density n_c, which is a function of the kinetic temperature and the ratio of the radiation and kinetic temperature,

$$n_c\left(T_e,\, \frac{T_{\rm rad}}{T_e}\right) = \frac{B}{A}\,\frac{y_e^{1/2}}{y_{\rm rad}} \exp\,(y_e - y_{\rm rad}) F(y_e,\, y_{\rm rad})\,. \tag{6}$$

1. *The corona case.*—Assumes that the radiation density is so small that photoionization is negligible compared to electron collision ionization, and the electron density is still so small that three-body recombination is negligible compared to radiative recombination:

$$n_c(T_e,\, 1) \gg n_e \gg W n_c(T_e,\, T_{\rm rad}/T_e)\,. \tag{7}$$

Hence, the departure coefficient can be approximated by

$$b_j \simeq \frac{B}{An_e}\,\frac{1}{y_e^{1/2}}\, F(y_e,\, y_e) = \frac{n_c(T_e,\, 1)}{n_e}\,, \tag{8}$$

which demonstrates that for coronal conditions the plasma becomes "underionized" to a degree smaller than the Saha equilibrium, and for which the ionization fraction becomes independent of the local electron number density, since it cancels out in equation (1) with equation (8).

2. *The Eddington case.*—Assumes that the electron density is so small that ionization is dominated by photoionization, and three-body recombination is dominated by radiative recombination:

$$n_c(T_e,\, 1) \gg n_e \quad \text{and} \quad W n_c(T_e,\, T_{\rm rad}/T_e) \gg n_e\,. \tag{9}$$

Hence, the departure coefficient can be approximated by

$$b_j \simeq \frac{1}{W}\,\frac{y_{\rm rad}}{y_e} \exp\,(y_{\rm rad} - y_e)\,\frac{F(y_e,\, y_e)}{F(y_e,\, y_{\rm rad})} \tag{10}$$

$$= \frac{1}{W}\,\frac{T_e}{T_{\rm rad}} \exp\left[\frac{I_j}{k}\left(\frac{1}{T_{\rm rad}} - \frac{1}{T_e}\right)\right]\frac{(1 - kT_e/I_j)}{(1 - kT_{\rm rad}/I_j)}\,. \tag{11}$$

Note that for these conditions of relatively low electron density and high radiation density, the ionization fraction still depends on the electron temperature through the radiative recombination mechanism.

2.2. *Governing Ionization Equation*

For our calculation of Γ_1 in the atmospheres of supergiants, we consider the Eddington approximation, for which photoionization dominates collisional ionization. The departures from LTE become very large in low-density, optically thin regions. Because of the radial variation of the local temperature and the wavelength variation of the opacity sources, the emitted spectrum departs from a blackbody at any particular temperature. However, for $T_{\rm eff}$ above 4000 K, the local gas density and temperature are only weakly determined by the ambient radiation field,

because important molecular opacity sources remain limited for these conditions. For our calculations we can assume that the stellar radiation field in the atmosphere where $\tau_{\rm Ross} < \frac{2}{3}$ (i.e., above R_*) can be approximated by the effective temperature, $T_{\rm rad} \simeq T_{\rm eff}$. For "gray" atmospheres in radiative equilibrium, the color (surface brightness or radiation) temperature is $0.811 T_{\rm eff}$ (Woolley & Stibbs 1953, p. 51).

We also consider non-LTE ionization conditions in atmospheric regions where $\tau_{\rm Ross} < \frac{2}{3}$, with T_e and $T_{\rm rad}$ below 20,000 K, for ionization energies I_j in excess of 7 eV. Hence, the trailing factor at the right-hand side of equation (11) approaches unity or

$$b_j \simeq \frac{1}{W} \frac{T_e}{T_{\rm rad}} \exp\left[\frac{I_j}{k}\left(\frac{1}{T_{\rm rad}} - \frac{1}{T_e}\right)\right]. \tag{12}$$

It represents a more tractable expression for our further derivation of important thermodynamic derivatives in § 4.2. The NLTE Saha equation in the Eddington approximation is hence obtained from equations (1), (2), and (12) for single ionization ($j = 0$–1) from the ground level (or $\chi_{r,j} = 0$) of element i:

$$\frac{n_i n_e}{n_0} = 2W \frac{u_{1,i}}{u_{0,i}} \left(\frac{2\pi m_e k T_{\rm rad}}{h^2}\right)^{3/2} \exp\left(-\frac{I_i}{k T_{\rm rad}}\right)\left(\frac{T_e}{T_{\rm rad}}\right)^{1/2}. \tag{13}$$

Eddington (1926) first considered ionization of the interstellar medium due to ionizing radiation from nearby stars, and obtained

$$\frac{n_i n_e}{n_0} = 2W \frac{u_{1,i}}{u_{0,i}} \left(\frac{2\pi m_e k T_{\rm rad}}{h^2}\right)^{3/2} \exp\left(-\frac{I_i}{k T_{\rm rad}}\right), \tag{14}$$

with $T_{\rm rad}$ of the order of the effective temperatures of stellar atmospheres. The factor on the right-hand side of equation (13), $(T_e/T_{\rm rad})^{1/2}$, is due to thermal motions, and first appears in Rosseland (1936). Strömgren (1948) gave a further refinement of equation (13) for photoionization from the ground state, which includes recombinations onto energy levels above the ground level. Weymann (1962) applied equation (13) in a study of the ionization equilibrium in the upper atmosphere of the supergiant α Ori (M2 Iab), where $T_e \leq$ 5500 K. Similar applications to the wind conditions of stellar chromospheres are given in, e.g., Hartmann & McGregor (1980).

We conclude this section by emphasizing that the condition of detailed balance, for photoionizations by an equal number of recombinations (per unit volume and unit time) in the Eddington approximation, is required for applying equation (13). In addition to the condition of detailed balance, our calculations of thermodynamic quantities also require that the kinetic temperatures of the neutrals, ions, and electrons thermalize on a timescale shorter than the characteristic timescale of heat exchange within the fluid; i.e., due to an atmospheric temperature gradient. The proton-electron relaxation time (Spitzer 1972) is

$$t_s(p, e) = \frac{3 m_p (2\pi)^{1/2} (k T_e)^{3/2}}{8\pi m_e^{1/2} n_e Z_p^2 e^4 \ln\Lambda} = \frac{503 A_p T_e^{3/2}}{n_e Z_p^2 \ln\Lambda} \ \text{s}, \tag{15}$$

where $Z_p = 1$ is the proton charge number, e is the electron charge, and A_p is the proton mass m_p in atomic units ($\simeq 1$). For $2 \times 10^3 \leq T_e \leq 2 \times 10^4$ K, in the atmospheres of supergiants, where $n_e \sim 10^{12}$ cm^{-3}, and which are mainly composed of hydrogen, we compute for $\ln\Lambda \simeq 10$ (as tabulated in Spitzer 1962) that large hydrodynamic perturbations of the local state variables should not occur on timescales shorter than $9 \times 10^{-7} \leq t_s \leq 5 \times 10^{-6}$ s, or on characteristic length scales smaller than $V_{\rm flow} t_s$. Equilibrium thermodynamic conditions cannot, for example, be established within the thin layer trailing strong shock waves where the electron temperature departs from the heavy particle gas temperature, or by the presence of strong electromagnetic fields that can separate the neutral and charged particle temperatures of a tenuous plasma.

3. STELLAR STABILITY COEFFICIENTS

Eddington (1918, 1919, 1926) first derived an analytical expression for the first adiabatic index Γ_1 for a mixture of material gas with radiation. His equation (129.52) is

$$\Gamma_1 = \beta + \frac{(4 - 3\beta)^2(\gamma - 1)}{\beta + 12(\gamma - 1)(1 - \beta)}, \tag{16}$$

where γ is the specific heat ratio, and β is the ratio of the material gas pressure to the total pressure (using modern symbols). He distinguished a general, or "effective," ratio of specific heats from the exponent to the density in the polytropic equation of state: $P = K\rho^{\Gamma}$, where K is a constant. Strictly thermodynamically speaking, the quantities Γ and Γ_1 are not identical, but the terminology of "an exponent" to indicate Eddington's adiabatic quantity

$$\Gamma_1 \equiv \left(\frac{\partial \ln P}{\partial \ln \rho}\right)_{\rm ad} \tag{17}$$

has been adopted since in the astrophysical literature. Eddington's consideration of evaluating *adiabatic* thermodynamic derivatives for studying adiabatic stellar oscillations was later more rigorously addressed by Chandrasekhar (1939). He defined the two other adiabatic indices,

$$\frac{\Gamma_2}{\Gamma_2 - 1} \equiv \left(\frac{\partial \ln P}{\partial \ln T}\right)_{\rm ad} \tag{18}$$

and

$$\Gamma_3 - 1 \equiv \left(\frac{\partial \ln T}{\partial \ln \rho}\right)_{\rm ad}, \tag{19}$$

and also first obtained detailed expressions for a mixture of material gas and radiation. Here P denotes the total pressure, i.e., the sum of partial material gas pressures and radiation pressure. Only two of the three adiabatic indices are independent, because a nondegenerate gas state is determined by at least two independent state variables,

$$\Gamma_3 - 1 \equiv \frac{(\Gamma_2 - 1)\Gamma_1}{\Gamma_2}. \tag{20}$$

With these definitions, Chandrasekhar also obtained more general expressions for the specific heats C_p and C_v, and clearly distinguished Γ_1 from C_p/C_v. His equation (148),

$$\Gamma_1 = \frac{C_p}{C_v} \beta, \tag{21}$$

where

$$C_p = \frac{c_p}{\gamma\beta^2}\,[\beta^2 + (\gamma - 1)(4 - 3\beta)^2 + 12(\gamma - 1)\beta(1 - \beta)] \tag{22}$$

and

$$C_v = \frac{c_v}{\beta}\,[\beta + 12(\gamma - 1)(1 - \beta)]\,, \tag{23}$$

where c_p and c_v are the specific heats of the material gas, marks an important step toward a self-consistent description of thermodynamic derivatives required in the theory of dynamical, convective, and pulsational stability of stellar atmospheres. Fowler & Guggenheim (1925) were the first to derive expressions for the specific heats with radiation, where various stages of ionization of the material are allowed. However, they made certain assumptions about the weight factors and the excitation of atoms and ions, which were too restricted. Independently, Möglich, Riewe, & Rompe (1939) derived expressions for the specific heats of a singly ionizing one-component monatomic gas without radiation, which were corrected shortly after by Biermann (1942). He calculated

$$c_p = \frac{Nk}{2}\,(1 + x)\left[5 + x(1 - x)\left(\frac{5}{2} + \frac{I}{kT}\right)^2\right] \tag{24}$$

and

$$c_v = \frac{Nk}{2}\,(1 + x)\left[3 + \frac{2x}{2 - x}\,\frac{1 - x}{1 + x}\left(\frac{3}{2} + \frac{I}{kT}\right)^2\right], \tag{25}$$

where I is the ionization energy, x is the ionization fraction, and N is the number of atoms per unit mass. Biermann also derived the correct expression for the first adiabatic index (evidently without using this terminology) for negligible radiation pressure,

$$\Gamma_1 = \frac{5 + x(1 - x)(5/2 + I/kT)^2}{3 + x(1 - x)[3/2 + (3/2 + I/kT)^2]}\,. \tag{26}$$

Note that the expression simplifies to equation (16) without partial ionization ($x = 0$), since $\beta \to 1$ with vanishing radiation pressure, and hence $\Gamma_1 \to \gamma = 5/3$ for monatomic gas.

Rosa & Unsöld (1948) extended the expressions for the specific heats by considering a mixture of partially ionizing hydrogen and helium gas. They also provided a detailed numerical evaluation of their expressions. These calculations followed an investigation by Unsöld (1938) of Schwarzschild's convection criterion. He improved on earlier work by Siedentopf (1933a, 1933b, 1935), and obtained the correct equation for the adiabatic temperature derivative,

$$\frac{\Gamma_2}{\Gamma_2 - 1} = \frac{5 + x(1 - x)(5/2 + I/kT)^2}{2 + x(1 - x)(5/2 + I/kT)}\,. \tag{27}$$

Unsöld (1938, p. 380) introduced the "mean" degree of ionization $\bar{x} = \sum_i^m \nu_i x_i$, where ν_i is the abundance of element i, and hence $\bar{x} = 1$ for a fully ionized gas. This enabled him to obtain an extended analytical expression for $\Gamma_2/(\Gamma_2 - 1)$ in terms of summations over the ionization fractions of m elements of a gas mixture (see his eq. [93, 20]). In the second edition of his monograph on stellar atmospheres, Unsöld (1968, p. 232) also derived an expression for c_p, by means of the definition of $\bar{x}$. A similar treatment for c_v is given in Menzel, Bhatnagar, & Sen (1963, p. 79). These equations, however, omit the important influence of a radiation field, as Chandrasekhar demonstrated. This problem has been investigated by Krishna-Swamy (1961), who computed the adiabatic temperature derivative for a multicomponent mixture of singly ionizing monatomic gas and radiation, using an equation of state of the form $P_t = NkT(1 + \bar{x})\rho + \frac{1}{3}aT^4$. The complete analytical expressions for the specific heats of this mixture were first derived by Mihalas (1965):

$$\begin{aligned}\frac{c_{P_t}}{Nk} = {} & \left(\frac{5}{2} + 20\alpha + 16\alpha^2\right) \\ & \times (1 + \bar{x}) + \sum_i \nu_i x_i(1 - x_i)\left(\frac{I_i}{kT}\right)^2 \\ & + \left(\frac{5}{2} + 4\alpha\right)\sum_i \nu_i x_i(1 - x_i)\,\frac{I_i}{kT} \\ & + \left[\frac{5}{2} + 4\alpha + \frac{\sum_i \nu_i x_i(1 - x_i)(I_i/kT)}{\bar{x} - \langle x^2\rangle}\right] \\ & \times \frac{\bar{x} - \langle x^2\rangle}{\bar{x}^2 - 2\bar{x} - \langle x^2\rangle} \\ & \times \left[\bar{x}(1 + \bar{x})\left(\frac{5}{2} + 4\alpha\right) - \sum_i \nu_i x_i(1 - x_i)\,\frac{I_i}{kT}\right], \end{aligned} \tag{28}$$

and

$$\begin{aligned}\frac{c_v}{Nk} = {} & \left(\frac{3}{2} + 12\alpha\right)(1 + \bar{x}) + \frac{3}{2}\sum_i \nu_i x_i(1 - x_i)\left(\frac{I_i}{kT}\right) \\ & + \sum_i \nu_i x_i(1 - x_i)\left(\frac{I_i}{kT}\right)^2 \\ & + \left[\frac{3}{2}\,\bar{x} - \sum_i \nu_i x_i(1 - x_i)\,\frac{I_i}{kT}\right] \\ & \times \frac{(3/2)(\bar{x} - \langle x^2\rangle) + \sum_i \nu_i x_i(1 - x_i)(I_i/kT)}{2\bar{x} - \langle x^2\rangle}\,, \end{aligned} \tag{29}$$

where $\langle x^2\rangle = \sum_i \nu_i x_i^2$, I_i is the ionization energy of element i, α is the ratio of the radiation pressure and the material gas pressure, and the other symbols have their usual meaning. These equations simplify to equations (24) and (25) in cases where the radiation pressure vanishes ($\alpha \to 0$), for a one-component gas $m = 1$ (hence $\bar{x} = x$ and $\langle x^2\rangle = x^2$). They also simplify to equations (22) and (23) when partial ionization of all elements vanishes ($x_i \to 0$), since $\alpha = 1/\beta - 1$, and for monatomic ideal gas $c_p = 5/2Nk$, $c_v = 3/2Nk$, or $\gamma = c_p/c_v = 5/3$. The analytical representation of equations (28) and (29) appears rather complex, but we show in § 4.2 that their further generalization, in which the gas temperature differs from the radiation temperature, enables us to define for every element i two functions G_i and H_i, which reduce c_{P_t} and c_v to basically two terms.

The calculation of the adiabatic indices for real gas in the context of equilibrium thermodynamics was first given by Cox & Giuli (1968, p. 183). The specific heat ratio is related to the ratio of the isothermal and adiabatic compressibility

coefficient via the Maxwell relations,

$$\frac{c_p}{c_v} = \frac{\kappa_T}{\kappa_S}, \tag{30}$$

with the coefficients

$$\kappa_T \equiv \left(\frac{\partial \ln \rho}{\partial P}\right)_T \quad \text{and} \quad \kappa_S \equiv \left(\frac{\partial \ln \rho}{\partial P}\right)_S, \tag{31}$$

where S denotes the thermodynamic entropy function. Hence, Γ_1 can be expressed by

$$\Gamma_1 \equiv \left(\frac{\partial \ln P_t}{\partial \ln \rho}\right)_S = \frac{c_{p_t}}{c_v}\left(\frac{\partial \ln P_t}{\partial \ln \rho}\right)_T. \tag{32}$$

The thermodynamic derivative, $(\partial \ln P_t/\partial \ln \rho)_T$, is the β factor on the right-hand side of equation (21), which Chandrasekhar distinguished from the specific heat ratio by calculating Eddington's index for a mixture of ideal material gas and radiation. Cox & Giuli (1968, p. 209) proposed calling this factor $(\partial \ln P_t/\partial \ln \rho)_T$ the "density exponent in the pressure equation of state" χ_ρ, probably following the adopted designation of "adiabatic exponent" for Γ_1;

$$\chi_\rho \equiv \left(\frac{\partial \ln P_t}{\partial \ln \rho}\right)_T, \quad \text{hence} \quad \Gamma_1 = \frac{c_{p_t}}{c_v}\chi_\rho. \tag{33}$$

Although this terminology has been widely adopted in the literature, we note that this quantity is by no means a true "exponent" in the polytropic equation of state. It is merely a coefficient to the specific heat ratio, required to determine an important adiabatic derivative. Fowler & Guggenheim (1925) also calculated this quantity and aptly called it "the isothermal factor" (see their eq. [9]), since it is inversely proportional to the isothermal compressibility coefficient: $\kappa_T = (P_t \chi_\rho)^{-1}$. Cox & Giuli (1968) also introduced the "temperature exponent" (more appropriately the "isochoric factor"),

$$\chi_T \equiv \left(\frac{\partial \ln P_t}{\partial \ln T}\right)_\rho, \tag{34}$$

which provides an important general relation for the thermodynamics of real gas:

$$c_{p_t} - c_v = \frac{P_t}{\rho T}\frac{\chi_T^2}{\chi_\rho}. \tag{35}$$

Thermodynamic stability demands that both heat capacities and both compressibilities are positive. For every real gas, $c_{P_t} > c_v$ and $\kappa_T > \kappa_S > 0$, and $c_{P_t} - c_v$ does not equal the universal gas constant. The latter equality applies only to simple ideal gas, for which $\chi_T = \chi_\rho = 1$.

With the definitions of the isothermal and isochoric factor, the two other adiabatic indices are obtained with

$$\frac{\Gamma_2}{\Gamma_2 - 1} = \frac{c_{P_t}}{c_{P_t} - c_v}\chi_T \tag{36}$$

and

$$\Gamma_3 - 1 = \frac{c_{P_t} - c_v}{c_v}\frac{\chi_\rho}{\chi_T}, \tag{37}$$

which yields the general identity equation (20). The complete expressions for χ_ρ and χ_T for a singly ionizing multicomponent monatomic gas with radiation are (Lobel et al. 1992)

$$\chi_\rho = \frac{\beta[\bar{x}^2 + \bar{x} + \sum_i \nu_i x_i(1 - x_i)]}{(1 + \bar{x})[\bar{x} + \sum_i \nu_i x_i(1 - x_i)]} \tag{38}$$

and

$$\chi_T = (4 - 3\beta) + \frac{\beta \bar{x} \sum_i \nu_i x_i(1 - x_i)(3/2 + I_i/kT)}{(1 + \bar{x})[\bar{x} + \sum_i \nu_i x_i(1 - x_i)]}. \tag{39}$$

Note that for a hypothetically nonionizing gas (x_i, $\bar{x}$) $\to 0$, and hence $\chi_\rho \to \beta$ and $\chi_T \to 4 - 3\beta$. These expressions simplify to those of Cox & Giuli (1968) for a gas composed of one ionizing element ($\bar{x} = x$) and radiation. Note that Biermann (1942) first derived χ_ρ without radiation ($\beta = 1$), but expressed as a factor to c_{P_t}/c_v,

$$\chi_\rho \equiv \left(\frac{\partial \ln P_t}{\partial \ln \rho}\right)_T = 1 - \left(\frac{\partial \ln \mu}{\partial \ln \rho}\right)_T = \frac{2}{(1 + x)(2 - x)}, \tag{40}$$

where μ is the mean molecular weight. In the partial ionization zone of an abundant element, the mean molecular weight reduces because $\mu = \mu_0/(1 + \bar{x})$, where μ_0 is the mean molecular weight of the un-ionized gas (e.g., $\mu_0 = 1.26$ for the abundance of cosmic material). In these regions the mean ionization fraction $\bar{x}$ increases ($0 \le \bar{x} \le 1$) and, as can be seen from equation (38), χ_ρ assumes values below unity. The increased compressibility in the thermal ionization regions reduces, with equation (32), the value of the first adiabatic index Γ_1 to below the monatomic gas value of 5/3. Here, compression energy is mainly converted into ionization energy, which also changes the local heat capacities. An equilibrium radiation field reduces $\beta \to 0$, and hence $\chi_\rho \to 0$ and $\chi_T \to 4$.

Lobel et al. (1992) demonstrated that Γ_1 can assume values *below unity* when isotropic radiation pressure is important in the partial ionization region of an abundant element, although $\gamma = c_{P_t}/c_v > 1$ for every stable gas. The higher compressibility of radiation, compared to pure material gas of the same temperature and pressure, diminishes χ_ρ to very low values for $6100 \le T_e \le 9000$ K, in the partial ionization region of hydrogen. Hence, Γ_1 can decrease to very small values of 0.84. Note, however, that when radiation vanishes, the product of the specific heat ratio and χ_ρ always exceeds unity ($\Gamma_1 \ge 1$). The extended equations (28), (29), (38), and (39) also enable us to correctly compute the compressibility of atmospheric regions where simultaneous ionizations of various elements (e.g., $H \to H^+$ and $He \to He^+$) considerably lower the values of Γ_1, Γ_2, and Γ_3.

The combination of ionization and radiation can diminish Γ_1 to below 4/3, which plays an important role in the study of dynamic stability of gas spheres, which we discuss in § 6. Conventional calculations of the adiabatic indices assume, however, that the gas and radiation temperature are equal, and that no interaction occurs between the material gas and the radiation field. We presently investigate the effects of a radiation field on the adiabatic indices due to photoionization in the Eddington approximation. The local ionization state is no longer determined by pure collisional processes, but by the incident and diluted radiation field as well. Radiative deviations from the Saha equilibrium produce important effects on the overall compressibility of the plasma, which directly determines the dynamic stability of supergiant atmospheres.

4. FIRST ADIABATIC INDEX WITH PHOTOIONIZATION

4.1. *Definition of the Generalized Functions*

When the radiation temperature differs from the local kinetic gas temperature, the classic equation of state, which assumes thermal equilibrium between material gas and radiation $P_t = NkT(1 + \bar{x})\rho + \frac{1}{3}aT^4$, is replaced by

$$P_t = NkT_e(1 + \bar{x})\rho + \frac{W}{3}\,aT_{\rm rad}^4\,, \tag{41}$$

where the first term is the material gas pressure, P_g, and the second term is the diluted radiation pressure, $P_{\rm rad}$. The gas state is hence determined by three independent state variables, instead of two. Therefore, the calculation of the first adiabatic index must consider T_e and $T_{\rm rad}$ as independent state variables. The constituent heat capacities,

$$c_{P_t} = \left(\frac{\partial h}{\partial T}\right)_{P_t} \quad \text{and} \quad c_v = \left(\frac{\partial e}{\partial T}\right)_{\rho}\,, \tag{42}$$

are replaced by

$$c_{P_t} = \left(\frac{\partial h}{\partial T_e}\right)_{P_t, T_{\rm rad}} + \left(\frac{\partial h}{\partial T_{\rm rad}}\right)_{P_t, T_e} \tag{43}$$

and

$$c_v = \left(\frac{\partial e}{\partial T_e}\right)_{\rho, T_{\rm rad}} + \left(\frac{\partial e}{\partial T_{\rm rad}}\right)_{\rho, T_e}\,, \tag{44}$$

where e denotes the internal energy function, and h is the enthalpy function. The lowercase symbols denote "specific" quantities, or expressed per unit mass. The isothermal factor

$$\chi_\rho = \left(\frac{\partial \ln P_t}{\partial \ln \rho}\right)_T \tag{45}$$

is replaced by

$$\chi_\rho = \frac{1}{P_t}\left[\left(\frac{\partial P_g}{\partial \ln \rho}\right)_{T_e} + \left(\frac{\partial P_{\rm rad}}{\partial \ln \rho}\right)_{T_{\rm rad}}\right]. \tag{46}$$

It is important to note that the three adiabatic indices become fully independent by the introduction of an additional state variable, $T_{\rm rad}$. Since the second and third adiabatic indices are temperature derivatives, they are also redefined by

$$\frac{\Gamma_{2,g}}{\Gamma_{2,g} - 1} \equiv \left(\frac{\partial \ln P_t}{\partial \ln T_e}\right)_{\rm ad}, \quad \frac{\Gamma_{2,\rm rad}}{\Gamma_{2,\rm rad} - 1} \equiv \left(\frac{\partial \ln P_t}{\partial \ln T_{\rm rad}}\right)_{\rm ad}\,, \tag{47}$$

and by

$$\Gamma_{3,g} - 1 \equiv \left(\frac{\partial \ln T_e}{\partial \ln \rho}\right)_{\rm ad}, \quad \Gamma_{3,\rm rad} - 1 \equiv \left(\frac{\partial \ln T_{\rm rad}}{\partial \ln \rho}\right)_{\rm ad}. \tag{48}$$

With these definitions, the identity equation (20) no longer applies, because it is only valid for thermodynamic systems with a unique temperature.

4.2. *Derivation of the Generalized Functions*

In the Appendix we obtain the detailed expression for the specific heat capacities for which T_e differs from $T_{\rm rad}$. The Appendix is self-contained and can be read without further cross-references. All thermodynamic quantities and functions are defined, and their detailed expressions are presented there. Major intermediate results, required to obtain the detailed expression for c_{P_t} and c_v, are also provided. We denote $\theta = T_e/T_{\rm rad}$, and find after considerable algebra

$$\frac{c_{P_t}}{Nk} = \left\{\frac{5}{2} + 4\alpha[4\theta(\alpha + 1) + 1]\right\}(1 + \bar{x}) + \sum_i v_i x_i(1 - x_i)H_i \tag{49}$$

and

$$\frac{c_v}{Nk} = \left(\frac{3}{2} + 12\alpha\theta\right)(1 + \bar{x}) + \sum_i v_i x_i(1 - x_i)G_i\,, \tag{50}$$

with the functions

$$X = \sum_i v_i x_i(1 - x_i)\,, \tag{51}$$

$$Y = \sum_i v_i x_i(1 - x_i)\,\frac{I_i}{kT_e}\,, \tag{52}$$

and for every element i,

$$Q_i = \frac{1}{2} + \theta\left(1 + \frac{I_i}{kT_{\rm rad}}\right), \tag{53}$$

$$G_i = Q_i\left[\frac{(3/2)\bar{x} - Y}{\bar{x} + X} + \frac{I_i}{kT_e}\right], \tag{54}$$

$$H_i = (Q_i + 1 + 4\alpha\theta) \times \left[\frac{(5/2 + 4\alpha)\bar{x}(1 + \bar{x}) - Y}{\bar{x}(1 + \bar{x}) + X} + \frac{I_i}{kT_e}\right]. \tag{55}$$

It can be shown that for $\theta = 1$, equations (49) and (50) simplify to equations (28) and (29). The first term in equations (49) and (50) is the heat capacity due to the translational motion of neutral atoms, ions, and electrons, and α is dependent on the diluted radiation pressure. The second term increases the heat capacities due to extra internal degrees of freedom, which result from partial photoionization by the incident radiation field. When $T_{\rm rad} \to T_e$, the NLTE ionization balance assumes the thermal Saha equilibrium, and the generalized heat capacities simplify to the heat capacities for a unique temperature T.

The analytical expression for the isothermal factor χ_ρ, in which $T_{\rm rad}$ differs from T_e, is formally identical to equation (38):

$$\chi_\rho = \frac{\beta[\bar{x}^2 + \bar{x} + \sum_i v_i x_i(1 - x_i)]}{(1 + \bar{x})[\bar{x} + \sum_i v_i x_i(1 - x_i)]}\,. \tag{56}$$

However, the dilution of the radiation pressure enters this generalized expression through β. The second term on the right-hand side of equation (46) vanishes because $P_{\rm rad}$ is invariable for constant $T_{\rm rad}$, and $P_{\rm rad}$ is independent of T_e. The derivative in the first term is evaluated for variable $T_{\rm rad}$, because the radiation temperature determines the NLTE ionization fraction.

In § 7 we investigate numerically the properties of the NLTE Γ_1 for multicomponent monatomic gas with radiation. If we consider only one element of material gas ($m = 1$ and $\bar{x} = x$), equation (49) simplifies to (see Lobel

1997, p. 83)

$$\frac{c_{P_t}}{Nk} = (1+x)\left\{\frac{5}{2} + 4\alpha[4\theta(\alpha+1)+1] + \frac{x(1-x)}{2}\left(\frac{5}{2} + \frac{I}{kT_e} + 4\alpha\right) \times \left[\frac{3}{2} + \theta\left(1 + \frac{I}{kT_{\rm rad}}\right) + 4\alpha\theta\right]\right\}, \quad (57)$$

and equation (50) to

$$\frac{c_v}{Nk} = \left(\frac{3}{2} + 12\alpha\theta\right)(1+x) + \frac{x(1-x)}{2-x}\left(\frac{3}{2} + \frac{I}{kT_e}\right)\left[\frac{1}{2} + \theta\left(1 + \frac{I}{kT_{\rm rad}}\right)\right]. \quad (58)$$

Because the isothermal factor equation (56) simplifies to

$$\chi_\rho = \frac{2\beta}{(1+x)(2-x)}, \quad (59)$$

we obtain after some algebra the NLTE "one-component" first adiabatic index,

$$\Gamma_1 = \frac{c_{P_t}}{c_v}\chi_\rho = \beta\left\{\frac{5}{2} + 4\alpha[4\theta(\alpha+1)+1] + \frac{x}{2}(1-x)\left(\frac{3}{2} + \Phi + 4\alpha\right)\left(\frac{3}{2} + \theta\Psi + 4\alpha\theta\right)\right\} \times \left\{\frac{3}{2} + 12\alpha\theta + \frac{x}{2}(1-x) \times \left[\left(\frac{1}{2} + \Phi\right)\left(\frac{1}{2} + \theta\Psi\right) + \frac{3}{2} + 12\alpha\theta\right]\right\}^{-1}, \quad (60)$$

where we denote

$$\Phi = 1 + \frac{I}{kT_e} \quad \text{and} \quad \Psi = 1 + \frac{I}{kT_{\rm rad}}. \quad (61)$$

For $T_e = T_{\rm rad} = T$, hence $\theta = 1$ and $\Phi = \Psi = 1 + I/kT$, it follows that equation (60) simplifies to (e.g., eq. [71.16] of Mihalas & Weibel Mihalas 1984)

$$\Gamma_1 = \beta\,\frac{5/2 + 20\alpha + 16\alpha^2 + (x/2)(1-x)(5/2 + I/kT + 4\alpha)^2}{3/2 + 12\alpha + (x/2)(1-x)[(3/2 + I/kT)^2 + 3/2 + 12\alpha]}, \quad (62)$$

which simplifies without radiation ($\alpha = 0$ and $\beta = 1$) to equation (26).

We have also obtained the detailed expressions for the two other adiabatic indices, Γ_2 and Γ_3, along similar lines, defined by equations (47) and (48), but these will be presented elsewhere. These generalized functions do not simplify to the classic expressions derived for a unique T, because the partial *temperature* derivatives, computed with the Saha equilibrium equation, differ from those obtained using the NLTE Saha equation. It should be remembered that the latter is an approximate expression for which the condition of detailed balance is assumed to sustain the condition of (ionization) equilibrium. The (LTE) Saha equation, however, is exact and follows from the minimization of the free energy function, which dictates the condition of thermodynamic equilibrium.

Note that for the computation of thermodynamic quantities, free energy minimization techniques have been applied to include the effects of pressure ionization due to Coulomb forces, and the effect of degenerate states (see Hummer & Mihalas 1988; Mihalas, Däppen, & Hummer 1988; Däppen et al. 1988). This numerical approach offers the advantage, for example, of incorporating the temperature dependency of the (properly truncated) internal partition functions, and of computing their effect on the heat capacities and the compressibilities. However, the free energy minimization scheme is strictly numerical, because a large system of nonlinear equations is to be solved iteratively for astrophysical mixtures (e.g., Mihalas et al. 1990).

In contrast, our formal approach for mixtures with simultaneously ionizing elements and $T_{\rm rad} \neq T_e$ offers the advantage of tracking analytically the complex behavior of the adiabatic indices. For example, consider the remarkable occurrence of conditions where $\Gamma_1 < 1$. Our formalism applies, however, to supergiant atmospheres, for which electrostatic interactions and degenerate states are negligible. Possibly, relativistic or degenerate gas effects on Γ_1 can be incorporated by the analytical approximations outlined in Cox & Giuli (1968), Beaudet & Tassoul (1971), Elliott & Kosovichev (1998), and Stolzmann & Blöcker (2000). Ecker & Kroll (1963) presented an interesting statistical method, based on the minimum entropy production principle of irreversible thermodynamics, to compute the lowering of ionization energy for a Saha-type equation that considers Coulomb interaction. Note also that Mollikutty, Das, & Tandon (1989) computed effects of a uniform magnetic field on the adiabatic indices, and provided generalized LTE expressions for the heat capacities, including the magnetic pressure.

4.3. *General Thermodynamic Relation for* Γ_1

We conclude this section with an important thermodynamic relation for Γ_1. From the first law, the relationship among P_t, ρ, and e along an isentrope ($dS = 0$) is

$$\left(\frac{d\ln e}{d\ln\rho}\right)_{\rm ad} = \frac{h}{e} - 1, \quad (63)$$

where $h = e + P_t/\rho$. The introduction of an additional state variable $T_{\rm rad}$ defines surfaces of constant (total) entropy with the specific entropy function $s = s(\rho, T_e, T_{\rm rad})$ in the space of three independent state variables. For adiabatic changes, $de = P_t/\rho^2 d\rho$ and $dh = 1/\rho dP_t$, the first adiabatic index can be expressed by

$$\Gamma_1 \equiv \left(\frac{d\ln P_t}{d\ln\rho}\right)_{\rm ad} = \left(\frac{dh}{de}\right)_{\rm ad}. \quad (64)$$

The value of Γ_1 is related to the slope along an adiabate in the (P_t, ρ) plane, for a given $T_{\rm rad}$ or T_e. Since the NLTE Saha equation considers local interactions of material gas with the incident radiation field, the total entropy function cannot classically be obtained by summing over the particle entropy fractions, the entropy of released electrons, and the entropy of equilibrium radiation (i.e., by means of the Sackur-Tetrode equation; see Lobel 1997, p. 83). Here

$s(\rho, T_e, T_{\rm rad})$ is to be obtained from the temperature derivative of the free energy, defined for the gas state determined by T_e *and* $T_{\rm rad}$. Similarly, for conditions of equilibrium, $e = e(\rho, T_e, T_{\rm rad})$ and $h = h(\rho, T_e, T_{\rm rad})$ are uniquely defined functions, and it can be shown that their ratio $\gamma_H = h/e$ is related to the first adiabatic index by

$$\Gamma_1 = \gamma_H + \frac{\gamma_H}{\gamma_H - 1}\left(\frac{d\ln\gamma_H}{d\ln\rho}\right)_{\rm ad} . \qquad (65)$$

Hence, the decrease of Γ_1 due to partial ionization and the release of bound electrons is related to the decrease of γ_H (e.g., Nieuwenhuijzen et al. 1993). While the value of Γ_1 is related to the adiabatic compressibility of the fluid (e.g., the bulk modulus) by local mechanic perturbations, the value of γ_H is determined by the corresponding changes of the internal energy.

5. BEHAVIOR OF Γ_1 IN SUPERGIANT ATMOSPHERES

Figure 1 shows the behavior of Γ_1 and the mean ionization fraction $\bar{x}$, for variable T_e and $T_{\rm rad}$. We compute the thermodynamic quantities for a mixture of 16 elements comprising H, He, C, N, O, Ne, Na, Mg, Al, Si, S, Ar, K, Ca, Cr, and Fe, for solar abundance values (Anders & Grevesse 1989). The internal partition functions are derived according the methods developed by Claas (1951) and by Baschek, Holweger, & Traving (1966). The left-hand panels of Figure 1 display the NLTE Γ_1 computed at the stellar radius ($W = \frac{1}{2}$), and the right-hand panels show $\bar{x}$. In the top panels the material gas pressure is set to 10 dyn cm^{-2}, whereas 0.5 dyn cm^{-2} is used for the bottom panels. These conditions are typical for the atmospheres of cool supergiants. Figure 1 reveals that Γ_1 acquires minimum values for $T_{\rm rad}$ between 7000 and 9000 K, primarily due to the partial ionization of hydrogen. Toward very low $T_{\rm rad}$, Γ_1 approaches the value of 5/3 for monatomic ideal gas, whereas for high $T_{\rm rad}$, Γ_1 assumes the equilibrium radiation value of 4/3. The intermediate regions with lowest Γ_1 correspond to $\bar{x} \simeq 0.5$. The NLTE ionization equation causes a strong dependence of the local mean ionization fraction on the value of $T_{\rm rad}$. For a given radiation temperature, however, at constant gas pressure, the ionization fraction *decreases* toward higher kinetic gas temperatures, because the NLTE ionization fraction remains dependent on the local kinetic temperature through the factor $T_e^{1/2}$ in equation (13) (but which is $T_e^{3/2}$ for pure collisional ionization).

We find minimum values for Γ_1 that can decrease to below 0.7 for very small gas pressures and low T_e. The minima gradually increase for larger gas pressures, by shifting toward higher $T_{\rm rad}$. This is also shown by the Γ_1 surface plots of Figure 2. The deep minimum around $T_{\rm rad} \simeq 8000$ K (*bottom panel*) becomes shallower and broadens for increased kinetic pressures (*top panel*). The relative decrease of the radiation pressure also enhances the partial ionization of He, which is visible for $T_{\rm rad}$ between 14,000 and 16,000 K. Note that we have also included the partial ion-

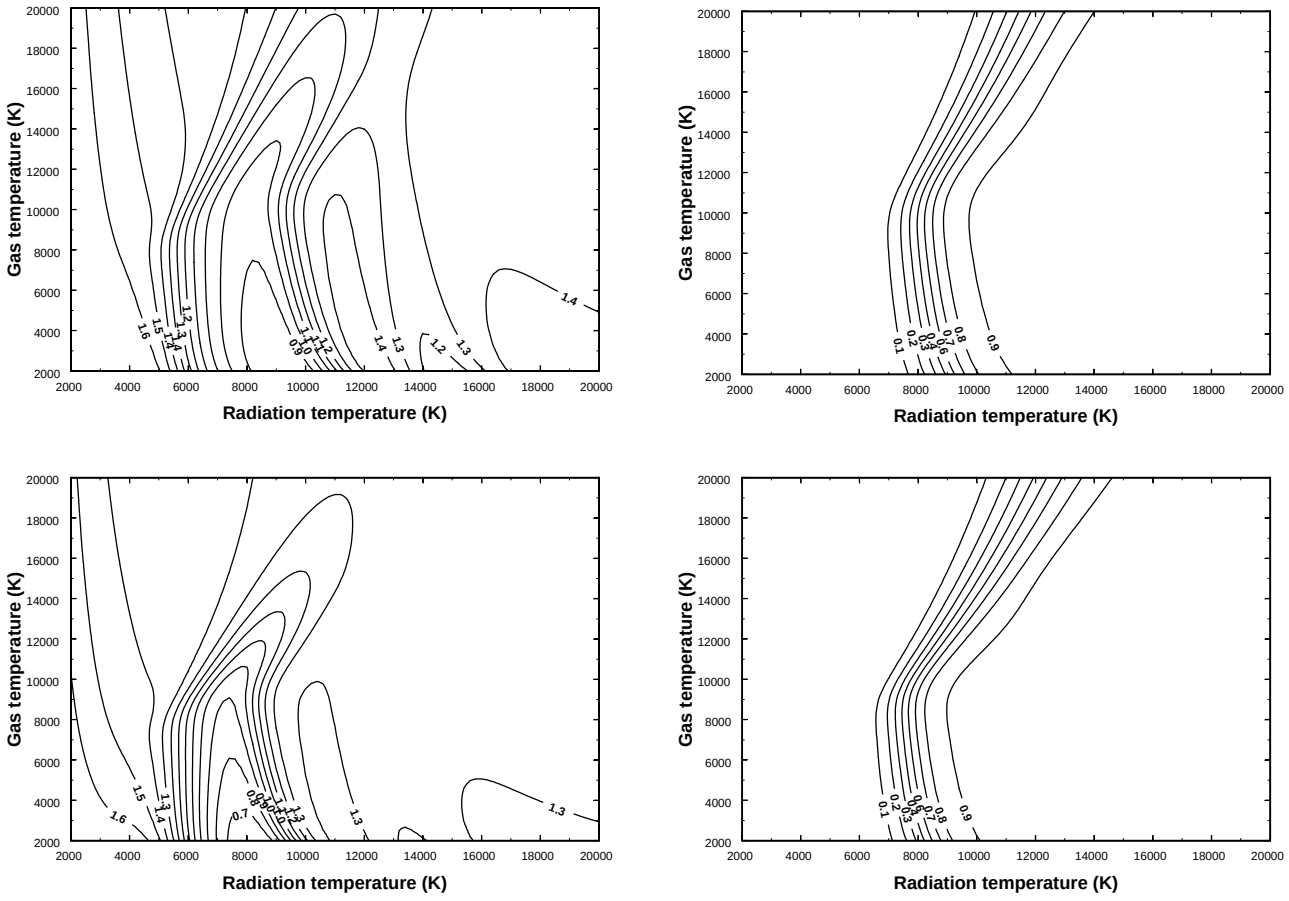

FIG. 1.—*Left*: First adiabatic index Γ_1 computed with partial NLTE ionization for conditions of cool supergiant atmospheres. The mean ionization fraction $\bar{x}$ (*right*) varies with the radiation temperature and the kinetic gas temperature (T_e). Here Γ_1 assumes minimum values for $\bar{x} \simeq 0.5$ toward smaller T_e. The top panels are for a gas pressure of 10 dyn cm^{-2}, and the bottom panels for $P_g = 0.5$ dyn cm^{-2}.

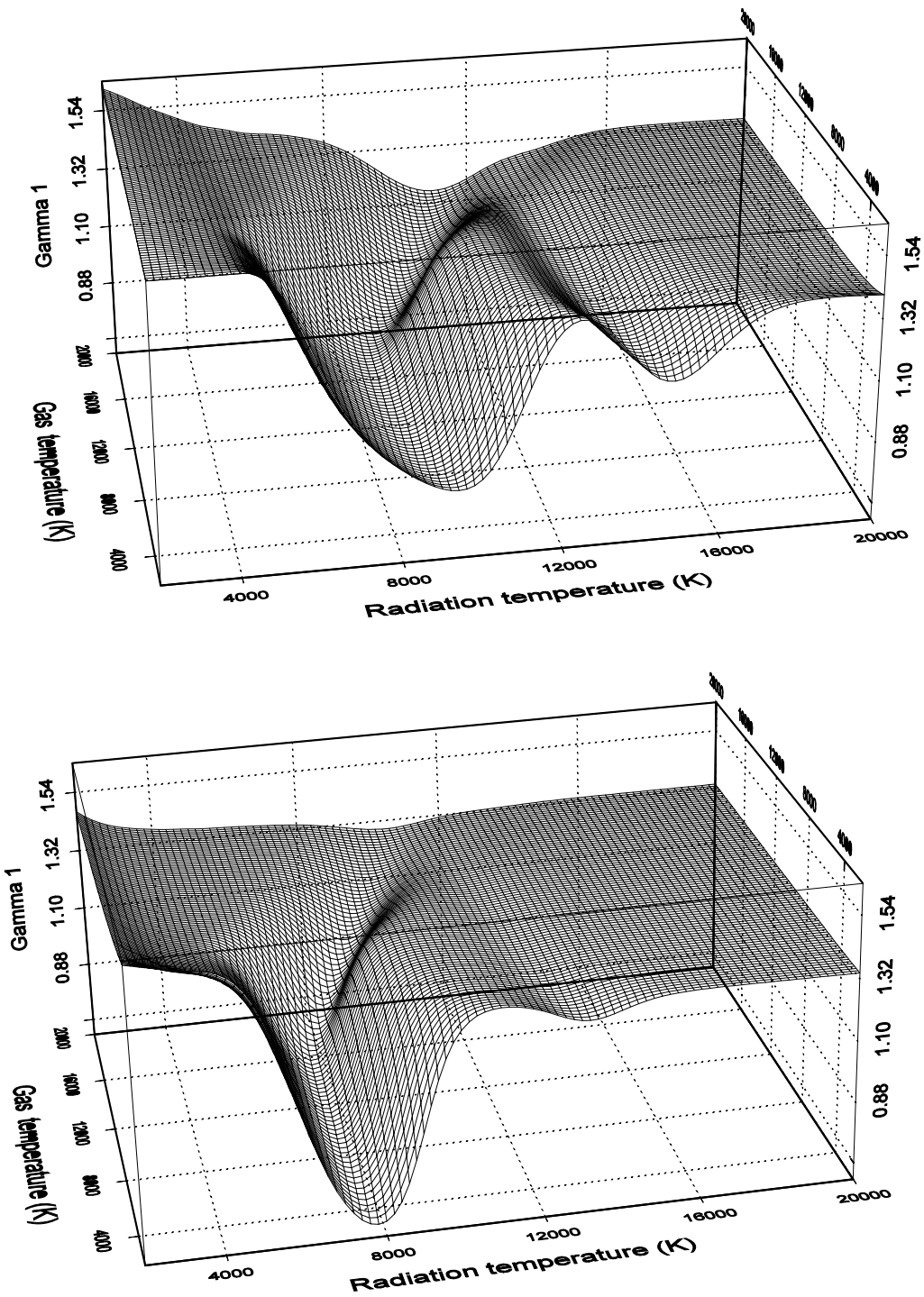

FIG. 2.—Γ_1 surface plots for $P_g = 10$ (*top*) and 1 (*bottom*) dyn cm^{-2}. The deep minima of Γ_1 result from partial NLTE ionization of hydrogen with $7000 \leq T_{\rm rad} \leq 9000$ K. The minima between 14,000 and 16,000 K result from the partial ionization of helium. The decrease of P_g yields smaller minima for Γ_1 with values below 0.7, which corresponds to very high gas compression ratios for these conditions in the atmospheres of cool supergiants.

ization of He^+ in our calculations. Its ionization can be treated as a separate "element," because the ionization energy is very high, and partial ionization occurs around 25,000 K for $P_g = 1$ dyn cm^{-2}. Electrons from less abundant metal atoms, with smaller ionization energies, contribute only slightly to the total electron pressure. The much larger abundance of hydrogen (by about a factor of 10 larger than the He abundance) causes the large decrease of Γ_1 to occur for $T_{\rm rad}$ between 7000 and 9000 K, for the small gas pressure conditions of supergiant atmospheres.

An important influence on the local mean ionization fraction is the dilution of radiation pressure with distance above R_*, which we further discuss in § 7.1. Calculations with $W(z) < \frac{1}{2}$ (for $z > 1$) reveal that the minima of Γ_1 increase, which is expected when kinetic pressure dominates the gas state.

6. THEORY OF STELLAR DYNAMIC STABILITY

The theory of adiabatic oscillation of gas spheres shows that, for homologous radial motion, the square of the angular frequency of the lowest radial pulsation mode, in the linear approximation, is given by (Ledoux 1945, 1965)

$$\sigma_0^2 = \frac{\int_0^R (3\Gamma_1 - 4)3P_t\,dV}{\int_0^R r^2\rho\,dV} = \left\langle \Gamma_1 - \frac{4}{3} \right\rangle \frac{3\Omega_0}{I_0}, \qquad (66)$$

where Ω_0 is the gravitational potential of the star in its equilibrium state, and I_0 denotes the moment of inertia with respect to the center of the star. Since Γ_1 is a function of depth in the star, the integration requires geometrical depths down to the stellar center for the computation of σ_0^2. When $\sigma_0^2 > 0$, the configuration is stable, because the standing-wave solution of the equation of motion does not grow with time. For supergiants, we can assume that the fundamental eigenfrequency σ_0 is not affected by magnetic fields, and that rotational kinetic energy can be neglected.

Stellar dynamic stability depends on the volume-averaged value of Γ_1, and vanishes when this average,

$$\langle \Gamma_1 \rangle = \frac{\int_0^R \Gamma_1 P_t\,dV}{\int_0^R P_t\,dV}, \qquad (67)$$

is less than 4/3, and hence $\sigma_0^2 \leq 0$. Because our detailed knowledge of Γ_1 is limited to the atmospheric layers, it is not straightforward to infer stellar dynamic stability from equation (67). However, Stothers (1999) recently argued that the integral can be limited to "an effective basis," or a point at which $\langle \Gamma_1 \rangle$ becomes constant in deeper parts of the atmosphere near the base of the stellar envelope. Numerical integrations of the equation of motion demonstrate that this truncation is allowed, because the radius eigenfunction $\delta(r)/r$ (the relative pulsation amplitude) at the base of the outer envelope is already many orders of magnitude smaller than its value at the stellar surface (so small that it is virtually indistinguishable from zero). Since regular stellar pulsation is caused by envelope mechanisms, this limitation of Ledoux' stability integral provides a useful means to test for atmospheric stability throughout the H-R diagram. Note, however, that a sound analytical foundation for this numerical "criterion" is currently lacking, and that important thermodynamic effects due to improved descriptions of Γ_1, as we present here, are crucial to ascertain its validity. Nevertheless, atmospheric regions where ionization and radiation cause Γ_1 to locally decrease to below 4/3 are of great interest. These real gas effects also influence Γ_2 and Γ_3 in supergiants (e.g., Lobel et al. 1992). It is well known that the local lowering of Γ_2 causes the onset of convective motions. Unsöld (1948) mentions convective "instability" regions in the partial ionization zones of H and He. For dynamically stable atmospheres, the local decrease of Γ_3 is linked to an increase or decrease of oscillation amplitudes over time, which determines the star's pulsational stability.

7. APPLICATION TO SUPERGIANT MODEL ATMOSPHERES

7.1. *Model Grid*

Based on the NLTE expression for Γ_1 in § 4.2, we investigate dynamic stability of atmospheric models we calculate for a range of effective temperatures and gravity accelerations for cool supergiants. The new model grid is computed to very high optical depths of $\log(\tau_{\rm Ross}) \simeq 5$ with ATLAS9 (R. Kurucz 2000, private communication). A modified version of ATLAS9 is used, which, for certain models, includes 999 optical depth points. The number of points per decade has been improved for the computation of numerical derivatives in the treatment of convection. In deep model layers, the convection decreases or completely vanishes.[1] The temperature structure for models with spherical symmetric geometry will change significantly, and more detailed solutions of the NLTE problem (i.e., by solving detailed rate equations) will influence the behavior of Γ_1. In the present application, we assume that the stellar radiation field in the optically thin part of the model atmospheres ($\tau_{\rm Ross} < \frac{2}{3}$) can be approximated by the stellar effective temperature for our computation of Γ_1 with height (see § 8 for a discussion).

The top panel of Figure 3 shows the behavior of Γ_1 (*bold solid line*) in the model with $T_{\rm eff} = 8000$ K and $\log g = 1.0$. In the partial NLTE ionization region of hydrogen, Γ_1 decreases to ~ 0.8, around $\log \tau_{\rm Ross} = -2$. Toward smaller $\tau_{\rm Ross}$, Γ_1 increases and assumes values of $\sim 4/3$ (*dotted horizontal line*) in the outermost atmospheric layers. This results

[1] More information on the ATLAS9 code and these plane-parallel hydrostatic models is available from Kurucz web site, http://kurucz/grids.html.

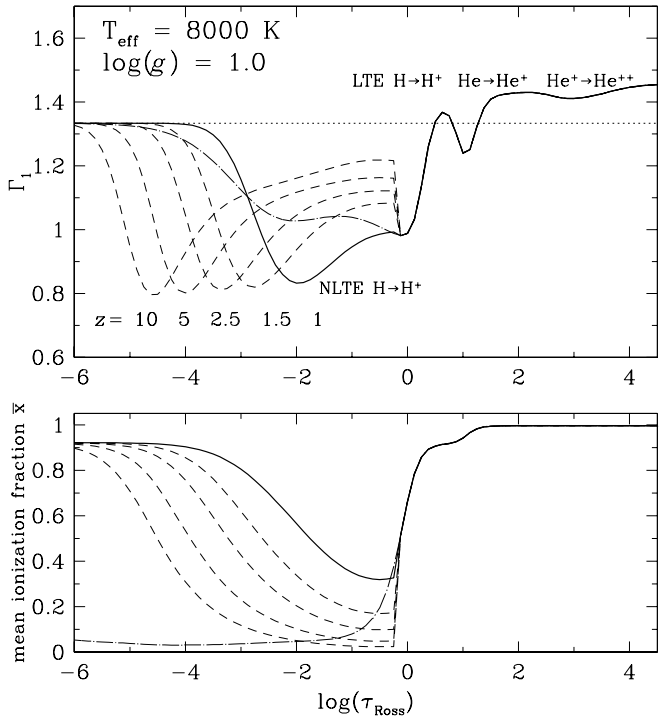

FIG. 3.—Run of Γ_1 in the model atmosphere with $T_{\rm eff} = 8000$ K and $\log g = 1.0$. The strong decrease of Γ_1 to below 4/3 (*dotted horizontal line*) results from partial NLTE ionization for optical depths $\tau_{\rm Ross} < \frac{2}{3}$ ($\sim R_*$; *bold solid line*). We assume $T_{\rm rad} = T_{\rm eff}$ and $W = \frac{1}{2}$ for the computation of Γ_1 above R_*. At larger depths in the photosphere, Γ_1 mainly decreases because of thermal (LTE) ionization of H and He. The corresponding mean ionization fraction $\bar{x}$ is shown in the bottom panel (*bold solid line*). At smaller optical depths the gas becomes fully ionized because $T_{\rm rad}$ exceeds T_e. For unrealistic conditions of LTE, with $T_{\rm rad} = T_e$, these layers would assume a very small $\bar{x}$, with larger Γ_1 values (*dash-dotted lines*). The influence of the dilution of radiation with distance z above R_* is shown by dashed lines. The mean ionization fraction assumes $\bar{x} \simeq 0.5$ at smaller optical depths when the ionizing radiation field dilutes more with increasing distance z. Consequently, the deep minimum of Γ_1 in the top panel, due to partial NLTE ionization of hydrogen, occurs at smaller optical depths.

from the ionizing stellar radiation field, which enhances the mean ionization fraction (*bottom panel*, *solid line*) of very optically thin layers. When only collisional ionization is considered (*dash-dotted line*), the local kinetic temperature becomes too low to appreciably partially ionize the fluid, and Γ_1 exceeds unity. The Γ_1 minimum is therefore determined by the incident stellar radiation field, which dilutes above R_* ($\tau_{\rm Ross} < \frac{2}{3}$). The influence of lowering $W(z)$ in the NLTE ionization equation and in the radiation pressure is shown by the dashed lines for different values of z. The dilution of the ionizing radiation field diminishes the local value of $\bar{x}$, and the point at which $\bar{x} \simeq 0.5$ occurs in layers of increasingly smaller optical depth. Hence, the corresponding minimum in Γ_1 (*top panel*) displaces toward smaller $\tau_{\rm Ross}$ values.

At large optical depths ($\tau_{\rm Ross} > \frac{2}{3}$), the radiation temperature approaches the kinetic gas temperature. Here Γ_1 decreases to below 4/3 due to thermal (LTE) ionization of hydrogen and helium, whereas a smaller decrease of Γ_1 results from He^+ ionization at the base of the model. At very large optical depths ($\tau_{\rm Ross} > 10{,}000$) we compute that the fluid becomes fully ionized, and Γ_1 assumes constant values around 1.45. Deeper down at the base of the stellar envelope, the value of Γ_1 asymptotically approaches 4/3, because radiation pressure outweighs the gas pressure for high temperatures above 10^5 K.

Figure 4 shows the behavior of Γ_1 in model atmospheres for $4000 \leq T_{\rm eff} \leq 20{,}000$ K, with small log g values. The models are plane-parallel and assume a constant value of 2 km s^{-1} for microturbulence with depth (Kurucz 1996). Although the effect of spherical geometry of extended atmospheres on the hydrostatic solution for the thermodynamic state is not negligible, we here compare differences in $T_{\rm rad}$ of at least 500 K, which are sufficient to outweigh this effect. We therefore infer global trends in Γ_1 for a wide range of effective temperatures. In the model with $T_{\rm eff} = 4000$ K (Fig. 4, *top left panel*), Γ_1 assumes values around 5/3 in the outer atmospheric regions. In deeper layers Γ_1 lowers to $\simeq 1.15$, primarily because of thermal (LTE) ionization of hydrogen. For $T_{\rm eff} = 5000$ K, the stellar radiation field

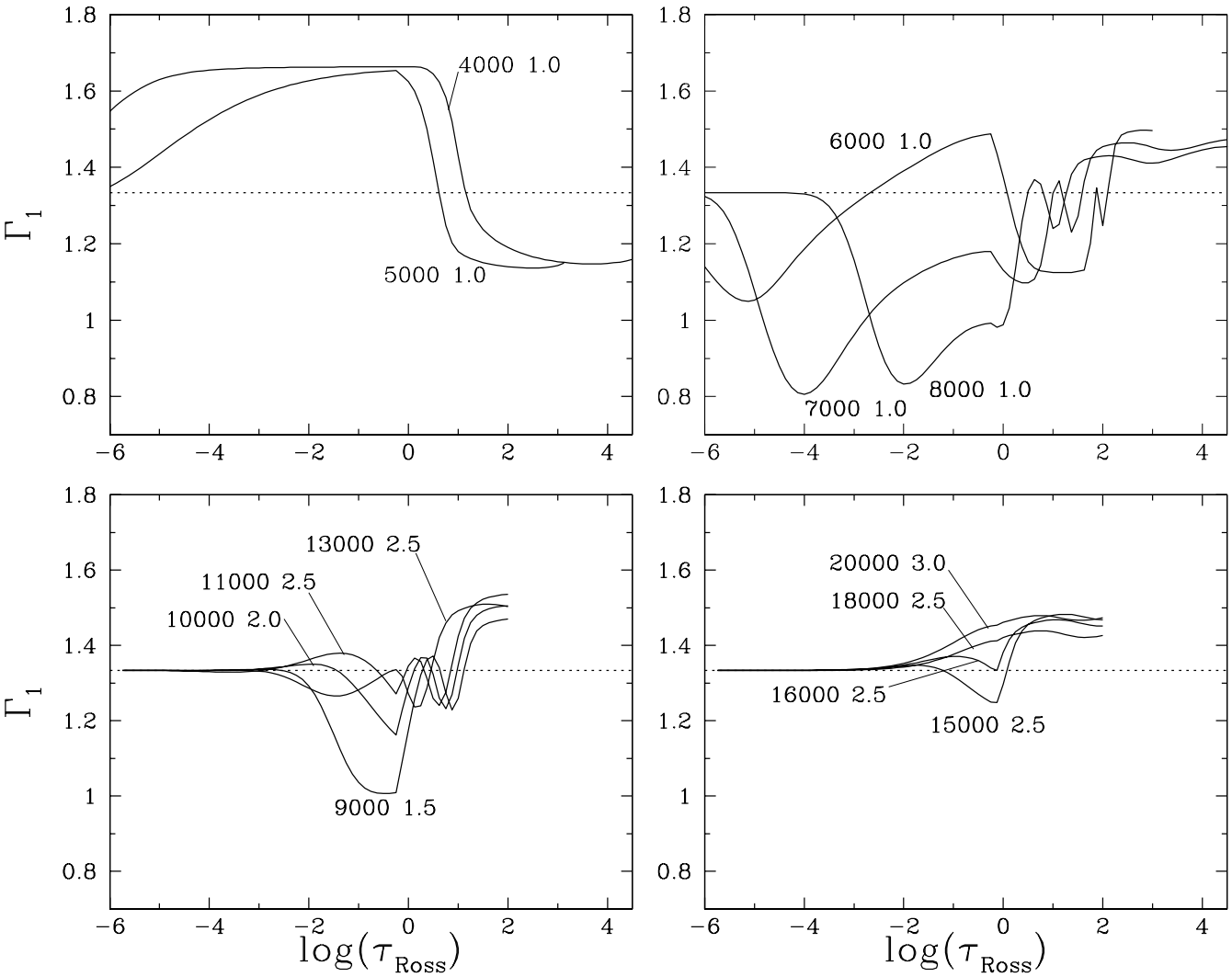

FIG. 4.—Behavior of Γ_1 in the outer envelope of supergiants with $4000 \leq T_{\rm eff} \leq 20{,}000$ K. Model $T_{\rm eff}$ and log g values are labeled. The NLTE Γ_1 assumes smallest values of ~ 0.8 above R_* ($\tau_{\rm Ross} < \frac{2}{3}$) for models with $T_{\rm eff}$ between 7000 and 8000 K (*top right panel*). We assume $T_{\rm rad} = T_{\rm eff}$ and $W = \frac{1}{2}$ for the computation of Γ_1 above R_*. Beneath R_*, the LTE Γ_1 values decrease to below 4/3 (*horizontal dotted lines*) because of partial ionization of H and He. These thermal ionization zones displace outward in models with higher $T_{\rm eff}$, while the partial hydrogen NLTE ionization region in the outer atmosphere displaces inward. This causes the deep Γ_1 minimum for $7000 \leq T_{\rm eff} \leq 8000$ K. Here Γ_1 assumes increasingly larger values for models of higher $T_{\rm eff}$ (*bottom panels*). For models with $T_{\rm eff} \geq 16{,}000$ K and log $g \geq 2.5$, helium is nearly fully ionized, and Γ_1 assumes values above 4/3 over the entire atmosphere (see text).

becomes sufficiently intense to partially photoionize hydrogen at very small optical depths, which strongly diminishes Γ_1. We set $W = \frac{1}{2}$ in our further calculations. When $T_{\rm eff}$ is increased to 6000, 7000, and 8000 K (Fig. 4, *top right panel*), we find that the partial photoionization region displaces toward *larger* optical depths. Here Γ_1 assumes very small local values of ~ 0.8 for models with $T_{\rm rad} = 7000$ and 8000 K. This results from the thermal ionization zone of hydrogen, but which displaces toward *smaller* optical depths for models with higher $T_{\rm eff}$. *This combined effect, whereby the partial thermal ionization zone displaces outward and the photoionization region displaces inward by raising* $T_{\rm eff}$, *causes* Γ_1 *to assume very small values* (*below unity*) *over a large geometrical fraction of supergiant models with* $7000 \leq T_{\rm eff} \leq 8000$ *K*.

In models with $9000 \leq T_{\rm eff} \leq 13{,}000$ K (Fig. 4, *bottom left panel*) we find that the minima in Γ_1 increase above R_*. This is because hydrogen becomes further ionized, or $\bar{x} > 0.5$ toward higher $T_{\rm rad}$. For the model with $T_{\rm eff} = 11{,}000$ K, hydrogen becomes nearly fully ionized, and Γ_1 exceeds 4/3 in the upper atmosphere. In these models the thermal He ionization region occurs at increasingly smaller optical depths, and for $T_{\rm eff} = 13{,}000$ K the region approaches $\tau_{\rm Ross} = \frac{2}{3}$ ($\sim R_*$). Around these effective (or radiation) temperatures, the partial photoionization zone of helium enhances in the upper atmospheric layers, and becomes noticeable by the decrease of Γ_1 to below 4/3. The bottom right-hand panel of Figure 4 shows the model with $T_{\rm eff} = 15{,}000$ K, in which the thermal and photoionization regions of helium merge, which reduces Γ_1 to ~ 1.25 around R_*. We find that atmospheric regions with Γ_1 below 4/3 are absent in models with $T_{\rm eff} > 16{,}000$ K. For the latter, the partial ionization of He^+ causes a minor decline in Γ_1, but which exceeds 4/3 throughout the entire model atmosphere.

7.2. *Model Gravity Dependence*

A comparison of Γ_1 for models with extended atmospheres reveals that their dynamic stability, according equation (67), strongly depends on $T_{\rm eff}$, or the ionizing stellar radiation field. However, differences in Γ_1 with depth in these models also depend on the gravity acceleration. Figure 5 shows the contour map of Γ_1 in the ($\log P_g$, T_e) plane. We compute Γ_1 with $T_{\rm rad} = T_{\rm eff}$ for models with 6000 (*top panel*), 8000 (*middle panel*), and 11,000 K (*bottom panel*), by setting $W = \frac{1}{2}$. For $T_{\rm eff} = 6000$ K, and P_g between 0.1 and 1 dyn cm^{-2}, the Γ_1 minima occur for $2000 < T_e < 8000$ K. This region marks the upper atmospheric layers where $-6 \leq \log \tau_{\rm Ross} \leq -4$ in the model with $\log g = 1.0$ (Fig. 4, *top right panel*). The filled diamonds in the top panel of Figure 5 show the ($\log P_g$, T_e) values of this model, while the filled triangles and squares are plotted for models with $\log g = 0.5$ and 0.0, respectively. The plots reveal that the Γ_1 values in layers of small optical depth and $T_e \leq 4000$ K are not dependent on $\log g$, and assume comparable values determined by the local gas pressure. However, in layers with $\tau_{\rm Ross} > \frac{2}{3}$, where $T_e > T_{\rm eff} = 6000$ K, Γ_1 assumes very different values ranging between 1.6 and 1.36, but which decrease toward smaller $\log g$ values. The same trend is noticeable in the Γ_1 contour map for $T_{\rm eff} = 8000$ K. The filled diamonds are shown for $\log g = 2.0$, the triangles for 1.5, and the squares for 1.0. Around $\tau_{\rm Ross} = \frac{2}{3}$ (where $T_e \simeq T_{\rm eff}$), Γ_1 decreases to below unity toward smaller $\log g$ values, as a result of enhanced partial photoionization of hydrogen. This also reveals that models computed for lower

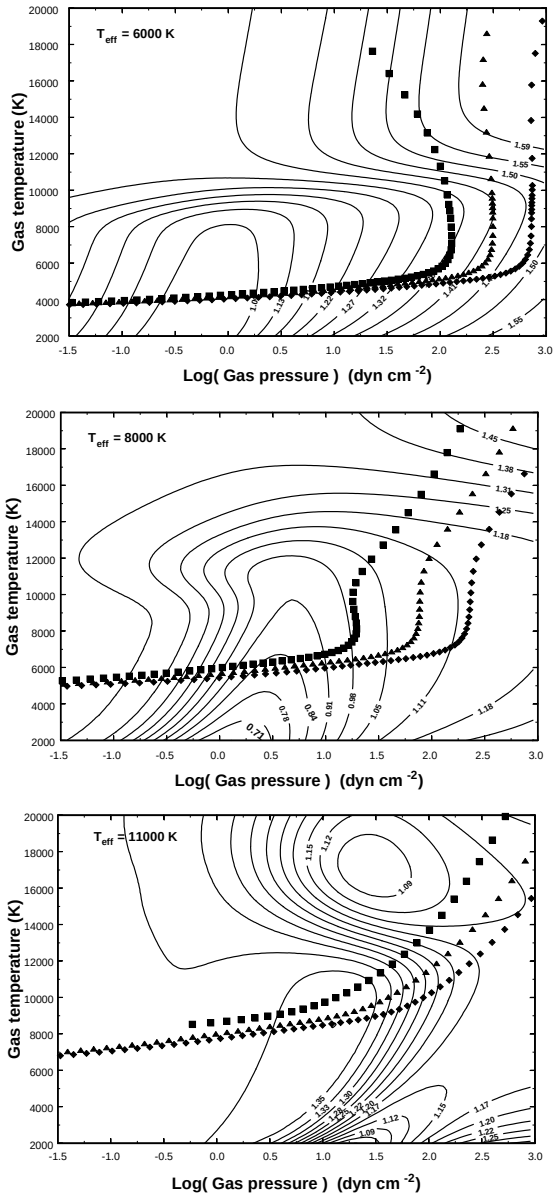

FIG. 5.—*Top*: Atmospheric models of supergiants with $T_{\rm eff} = 6000$ K plotted in the ($\log P_g$, T_e) plane, for three gravity accelerations of $\log g = 1.0$ (*diamonds*), 0.5 (*triangles*), and 0.0 (*squares*). The solid lines show the contour map of Γ_1, computed with NLTE for $T_{\rm rad} = T_{\rm eff}$ and $W = \frac{1}{2}$. The run of Γ_1 in the outer atmospheric layers, with $T_e \simeq$ 4000–5000 K, is very similar. The models differ more in the deeper layers, where different NLTE Γ_1 values are assumed. In layers with $T_e \simeq T_{\rm eff}$ (around R_*), Γ_1 decreases toward smaller $\log g$ values because the lines of equal Γ_1 decrease parallel with the local ($\log P_g$, T_e) structure. In deeper layers (below R_*), where $T_e > T_{\rm eff}$, Γ_1 values evaluated with NLTE ionization stay above 4/3. In these layers, LTE ionization calculations with $T_{\rm rad}$ set equal to T_e are required. *Middle*: Three models with $T_{\rm eff} = 8000$ K, plotted for $\log g = 2.0$ (*diamonds*), 1.5 (*triangles*), and 1.0 (*squares*). The NLTE Γ_1 contour map is computed for $T_{\rm rad} = 8000$ K. In layers near R_* ($T_e \simeq T_{\rm eff}$), Γ_1 assumes values below 4/3. The map reveals that in models with $\log g$ below 1.0 these layers will assume even smaller Γ_1 values, because their Γ_1 contours run parallel with the ($\log P_g$, T_e) lines. Stable hydrostatic solutions cannot be computed for these small gravity accelerations. *Bottom*: Three models with $T_{\rm eff} = 11{,}000$ K, plotted for $\log g = 3.0$ (*diamonds*), 2.5 (*triangles*), and 2.2 (*squares*). In layers near R_* ($T_e \simeq T_{\rm eff}$) the Γ_1 contour map varies perpendicular to the atmospheric structure variations with gravity of the models. The layers above R_* assume Γ_1 values around 4/3. Since hydrogen becomes nearly fully ionized, the upper atmospheres are more stable compared to the models with $T_{\rm eff} = 6000$ and 8000 K.

log g values would assume even smaller Γ_1 values in the optically thin region of the atmosphere. However, for log g values below 1.0 we could not converge models to a hydrostatically stable solution with $T_{\rm eff} = 8000$ K. This results from the outward-directed radiation pressure, which strongly increases the atmospheric density scale height with smaller gravity acceleration, and which reduces $\langle\Gamma_1\rangle$ to below 4/3. In the next section we show that the $\langle\Gamma_1\rangle$ integral yields the atmospheric gravity values for which hydrostatic models of a given $T_{\rm eff}$ become unstable.

The bottom panel of Figure 5 shows the Γ_1 contour map for $T_{\rm eff} = 11{,}000$ K. The partial hydrogen ionization region, with small Γ_1 values, occurs at high kinetic pressures of log $P_g \simeq 1.5$, because of the increased radiation temperature. The decrease of Γ_1 in the partial ionization region of helium is also noticeable at these pressures around $T_e \simeq$ 16,000 K. Three atmospheric models are plotted for log $g = 3.0$ (Fig. 5, *diamonds*), 2.5 (*triangles*), and 2.2 (*squares*). However, the latter has been extrapolated from the former two models. The detailed contour map reveals that the extrapolation does not lower Γ_1 to appreciably smaller values (i.e., to below unity) in the atmosphere. This results from hydrogen becoming nearly fully ionized by the incident radiation field, whereby Γ_1 assumes values around 4/3, also shown in the bottom left panel of Figure 4.

7.3. *Stability of Model Atmospheres*

We evaluate $\langle\Gamma_1\rangle$ for our grid of model atmospheres. With $dV = -d\rho/\rho^2$, equation (67) transforms to

$$\langle\Gamma_1\rangle = \frac{\int_{\rho_{\rm R}}^{\rho_*} \Gamma_1 (P_t/\rho) d\ln\rho}{\int_{\rho_{\rm R}}^{\rho_*} (P_t/\rho) d\ln\rho}, \tag{68}$$

where $\rho_{\rm R}$ is the density of the outermost atmospheric layer, and ρ_* is the density at the base of the stellar envelope. In layers of very high optical depth, beyond the partial H and He ionization zones, Γ_1 becomes locally constant, and $\langle\Gamma_1\rangle$ assumes an almost constant value. The models are dynamically stable against radial mechanic perturbations when $\langle\Gamma_1\rangle$ exceeds 4/3. In general, we find that this condition is valid for models that we can converge to a stable solution. However, toward smaller log g, $\langle\Gamma_1\rangle$ can decrease to values very close to 4/3.

Figure 6 shows the run of Γ_1 with log $\tau_{\rm Ross}$ (*thin solid lines*). The corresponding changes in $\langle\Gamma_1\rangle$ (*thick solid lines*) are shown by integrating over the atmosphere with equation (68) to the density at this optical depth. The atmospheric density structure of these cool supergiants is also shown for different log g values of 0.5 (*solid lines*), 1.0 (*short-dash-dotted lines*), 1.5 (*long-dashed lines*), and 2.0 (*long-dash-dotted lines*). For these small gravity accelerations, density inversions occur by the increase of continuum opacity in the hydrogen ionization region, which causes the outward-directed radiative pressure gradient to exceed the gravitational pull. The condition of hydrostatic equilibrium therefore requires an outward-increasing kinetic pressure (for a review see Maeder 1992). Pressure inversions occur in our models with $5250 \leq T_{\rm eff} \leq 8250$ K and $0.0 \leq \log g \leq 1.5$. The density-inversion layers occur at smaller optical depth with increasing $T_{\rm eff}$, because the thermal hydrogen ionization region displaces outward.

Our calculations demonstrate that NLTE ionization of hydrogen in the upper atmospheric layers of cool and extended atmospheres strongly diminishes $\langle\Gamma_1\rangle$ to below 4/3. The value of $\langle\Gamma_1\rangle$ at a given depth point in Figure 6 is a measure of the dynamic stability of the entire atmosphere above this point. A comparison of atmospheric conditions for different $T_{\rm eff}$ between 5500 and 8500 K reveals that changes in the radiation temperature by 1000 K strongly influence the behavior of $\langle\Gamma_1\rangle$ with depth. The partial NLTE ionization region of hydrogen displaces to higher depths by raising $T_{\rm eff}$ from 5500 to 6500 K (Fig. 6, *top panels*). The minimum of Γ_1 moves deeper into the atmosphere, and consequently $\langle\Gamma_1\rangle$ assumes smaller values around these depths. An integration of our model with $T_{\rm eff} = 6500$ K and log $g = 0.5$ to higher depths yields a strong decrease of $\langle\Gamma_1\rangle$ to below 4/3 around log $\tau_{\rm Ross} =$ 1.5 (*top right panel*). This partly results from the density inversion that occurs around these depths. The stability integral equation (68) is determined by the local behavior of Γ_1 *and* the atmospheric pressure and density structure. Toward larger optical depths $\langle\Gamma_1\rangle$ increases rapidly, because Γ_1 assumes local values above 4/3 (*dotted horizontal line*), and the density increases steeply. Above $\tau_{\rm Ross} \simeq$ 1000, the stability integral assumes almost constant values of $\simeq$1.37 at the base of the stellar envelope. The integration reveals that this supergiant model, with very low gravity acceleration, is dynamically stable, because the deeper envelope strongly contributes to the overall stability integral. However, we could not converge a model with $T_{\rm eff} =$ 6500 K and a smaller log g of 0.3 to a stable solution. Models with very small gravity yield $\langle\Gamma_1\rangle$ values below 4/3 when integrating equation (68) to the base of the stellar envelope.

Toward higher $T_{\rm eff}$ of 7500 K (Fig. 6, *bottom left panel*) we compute that the minimum of Γ_1 due to NLTE ionization displaces farther down the atmosphere, whereas the thermal H and He ionization regions occur at lower densities, higher in the atmosphere. However, in this model of higher $T_{\rm eff}$, but for the same log $g = 0.5$, the gas density and pressure also diminish. Therefore, the inward integration of the local Γ_1 causes a smaller decrease for $\langle\Gamma_1\rangle$ at comparable optical depths, although Γ_1 assumes locally very small minimum values of $\sim$0.8. On the other hand, we find that by integrating this model of increased $T_{\rm rad}$ to very high depths at the base of the envelope yields a $\langle\Gamma_1\rangle$ value of 1.34, or only marginally above 4/3. Stable models with log g below 0.5 could not be converged because $\langle\Gamma_1\rangle$ falls to below 4/3 in the deepest layers. In general, we find that models with increased $T_{\rm eff}$ (or $T_{\rm rad}$) become unstable toward higher gravity values because $\langle\Gamma_1\rangle$ drops to below 4/3. For $T_{\rm eff} =$ 8000 K a stable solution is possible when only log $g \geq 1.0$ (Fig. 6, *bottom right panel*), whereas for $T_{\rm eff} = 5500$ K we can converge stable models for log $g \geq 0.0$.

7.4. *Atmospheric Instability Regions in Cool Supergiants*

Stable models of the same gravity toward higher $T_{\rm eff}$ yield smaller $\langle\Gamma_1\rangle$ values at the base of the atmosphere, which is noticeable by comparing the four panels of Figure 6. For a given $T_{\rm eff}$ the stability integral increases with log g, which demonstrates that the deeper regions of compacter models have a strong influence by stabilizing the overlying atmosphere. Toward very high log g values, the gravity pull effectively balances the radiation pressure gradient, and the density inversion region vanishes. However, our NLTE calculations of $\langle\Gamma_1\rangle$ reveal a remarkable property: $\langle\Gamma_1\rangle$ assumes very small values, around unity, down to the base of the atmosphere (up to $\tau_{\rm Ross} \simeq 100$) for models with $T_{\rm eff}$

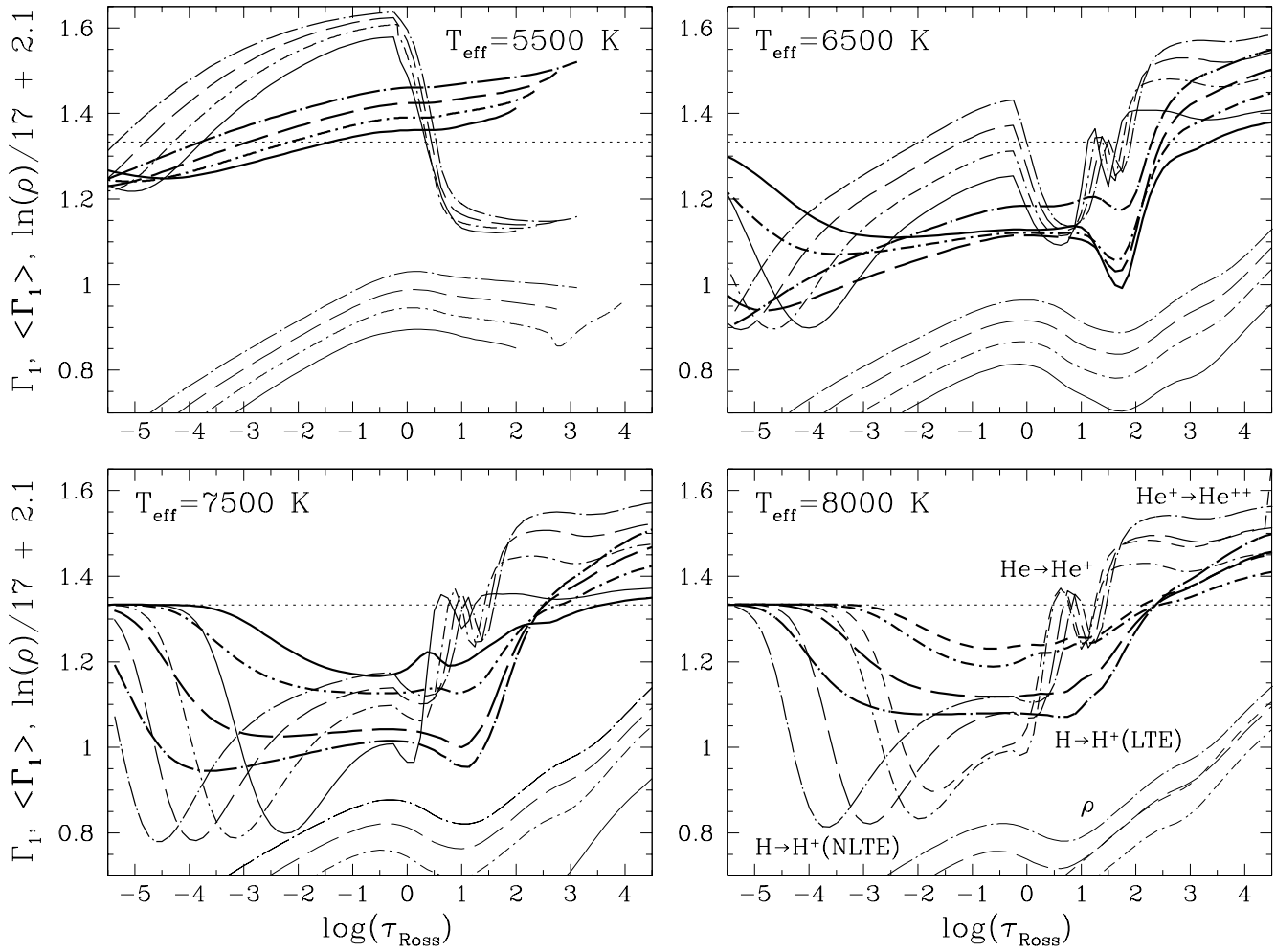

FIG. 6.—Behavior of Γ_1 (*thin lines*) and $\langle\Gamma_1\rangle$ (*bold lines*) with optical depth in envelope models of cool supergiants for different gravity accelerations. Here $\langle\Gamma_1\rangle$ is integrated to the density at the corresponding optical depth. We assume $T_{\rm rad} = T_{\rm eff}$ and $W = \frac{1}{2}$ for the computation of Γ_1 above R_*. Higher gravity models are more stable because $\langle\Gamma_1\rangle$ increases for a given $T_{\rm eff}$ at the base of the envelope with increasing log g = 0.5 (*solid lines*), 1.0 (*short dash-dotted lines*), 1.5 (*long-dashed lines*), and 2.0 (*long-dash-dotted lines*). For a given log g, toward higher $T_{\rm eff}$, $\langle\Gamma_1\rangle$ decreases at the base of the envelope to values close to 4/3 (*dotted horizontal line*). Models with log $g < 1.0$ are unstable for $T_{\rm eff} > 8000$ K. The model with $T_{\rm eff} = 8500$ K and log $g = 1.5$ (*bottom right panel, short-dashed lines*) is also shown. The partial ionization zones of hydrogen and helium, where Γ_1 locally decreases, are labeled. For $T_{\rm eff} = 6500$ and 7500 K, $\langle\Gamma_1\rangle$ assumes minimum values down to the base of the atmosphere (log $\tau_{\rm Ross} \sim 1.5$) due to partial NLTE and LTE H and He ionization, combined with the density- and pressure-inversion regions of these models. Note the near gravity independence for these minima in the models with $T_{\rm eff} = 6500$ K (see text).

around 6500–7500 K, practically independent of log g. Models with higher or lower $T_{\rm eff}$ (of the same gravity), yield *larger* $\langle\Gamma_1\rangle$ values at these depths, or they have more stable atmospheres.

To compare the run of Γ_1 and $\langle\Gamma_1\rangle$ in models of different $T_{\rm eff}$ and gravity, we plot the density scale in Figure 7, rather than optical depths. The thin drawn lines show Γ_1, with the deep minimum due to NLTE ionization of hydrogen, whereas the smaller minima at higher densities are due to the LTE ionization zones. The curious loops in this scale result from the density inversion for $\ln\rho$ between -24 and -20. The darker lines show the corresponding depression in $\langle\Gamma_1\rangle$ for models with log $g = 0.5$ (*solid lines*) and log $g = 1.0$ (*dashed lines*). For the latter, $\langle\Gamma_1\rangle$ assumes the smallest minimum of $\simeq 1.1$ for $\ln\rho \simeq -24$, around $T_{\rm eff} =$ 6500 K. In contrast, the value of $\langle\Gamma_1\rangle$ at the base of the model exceeds 4/3 ($\ln\rho > -19$), but it decreases steadily by further raising $T_{\rm eff}$ in steps of 500 K. In other words, the base of these supergiant models becomes less stable toward $T_{\rm eff}$ above 6500 K, whereas their extended atmospheric portions at lower densities tend to become more stable. The latter is also true for models with $T_{\rm eff}$ below 6500 K, but instead the deeper envelope further stabilizes the entire model.

Similar trends occur for models with log $g = 0.5$. We have incorporated the stronger dilution of radiation in these more extended atmospheres by setting $z = 1.5$, or the geometric dilution factor $W = (3 - \sqrt{5})/6$ (with eq. [5]) instead of $\frac{1}{2}$, for the calculation of Γ_1 above R_*. The minimum in Γ_1 therefore displaces toward smaller depths (see § 7.1), because partial ionization of hydrogen due to the more diluted radiation field occurs at lower densities. Consequently, $\langle\Gamma_1\rangle$ assumes smaller values at lower densities. Our calculations reveal that for models with smaller gravity, the minimum of $\langle\Gamma_1\rangle$ occurs for lower densities, and vice versa. The dilution of radiation tends to further destabilize a more extended atmosphere above R_*. In deeper layers where $T_{\rm rad} = T_e$, the atmosphere stabilizes because $\langle\Gamma_1\rangle$ increases, but assumes a smaller value above 4/3 (at the base of the envelope) than for models with higher

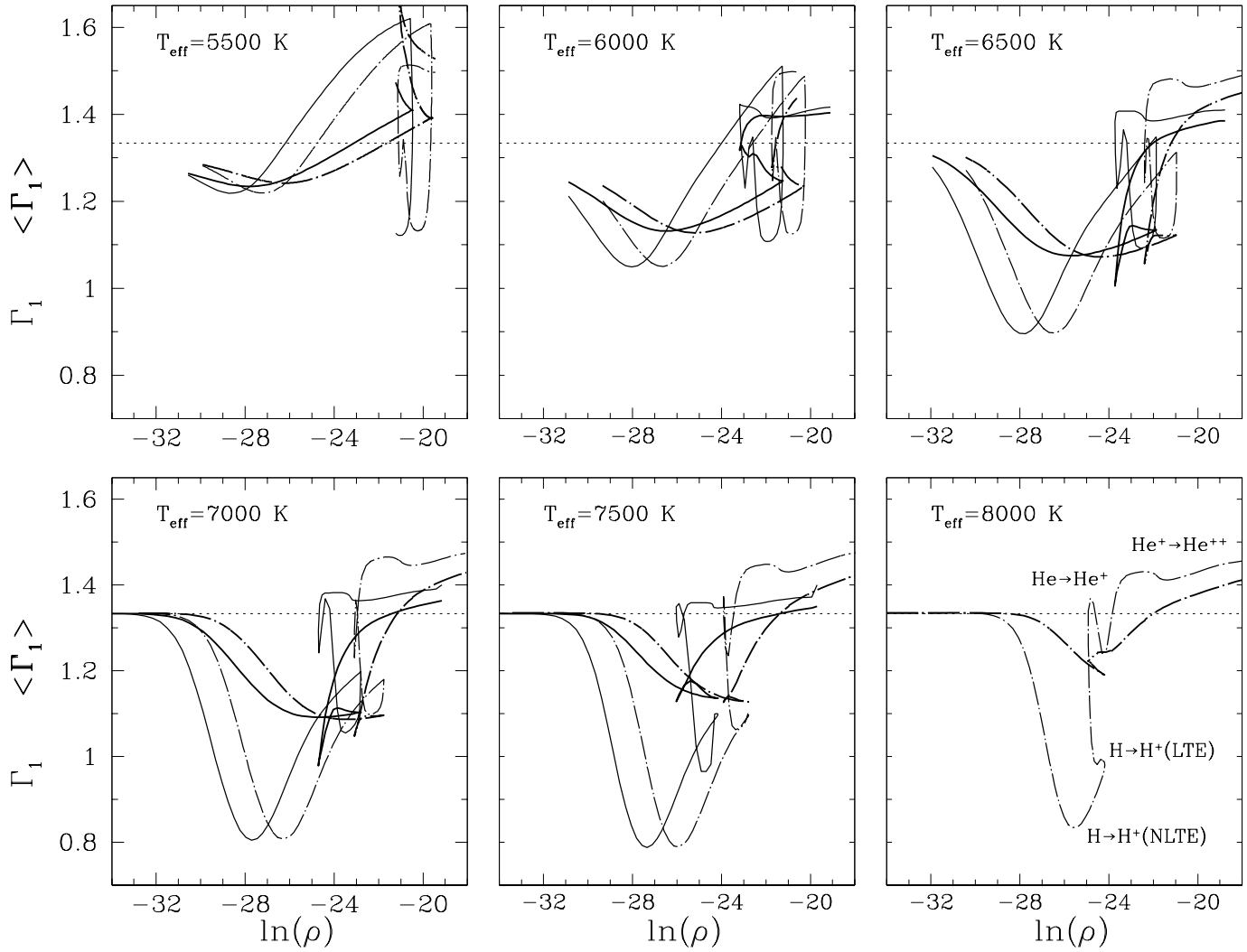

FIG. 7.—Run of Γ_1 (*thin lines*) and $\langle\Gamma_1\rangle$ (*bold lines*) in the atmospheric density scale for log $g = 0.5$ (*solid lines*) and 1.0 (*dash-dotted lines*). $\langle\Gamma_1\rangle$ assumes minimum values (below 4/3) in the atmosphere of stable models with $6500 \leq T_{\rm eff} \leq 7500$ K. We assume $T_{\rm rad} = T_{\rm eff}$ for the computation of Γ_1 above R_*. Toward smaller gravity acceleration the destabilizing regions, because of partial NLTE ionization of hydrogen, occur at lower density with the dilution of the ionizing radiation field (see text).

gravity. Lower gravity models are less stable, and the regions that contribute to their destabilization occur at smaller densities in the atmosphere. These regions contribute most strongly in supergiants with $6500 \leq T_{\rm eff} \leq 7500$ K, as the result of partial non-LTE ionization of hydrogen with $T_{\rm rad} \simeq T_{\rm eff}$ and the partial LTE ionization of hydrogen and helium, combined with the complex mean density and pressure structure of such extended atmospheres.

8. DISCUSSION

In a study of the evolution of luminous blue variable (LBV) stars Stothers & Chin (1994) evaluated $\langle\Gamma_1\rangle$ in the outer part of the stellar envelope and found that massive stars, evolving off the main sequence, develop dynamically unstable outer layers, for which eruptive mass loss can result. Humphreys & Davidson (1994) pointed out that the low surface temperature of 12,000 K at which the first instability occurs in these calculations appears to be underestimated, because of the absence of very luminous late B- or A-type stars. We note that LTE calculations for our model with $T_{\rm eff} = 12{,}000$ K and log $g = 2.0$ indeed show a decrease of Γ_1 to below 4/3 over a large fraction of the atmosphere with $\tau_{\rm Ross} < \frac{2}{3}$ (see Fig. 5 of Lobel et al. 1992). Toward higher $T_{\rm eff}$, hydrogen fully thermally ionizes, and hence Γ_1 increases above 4/3. However, our present NLTE calculations of Γ_1 show that stable supergiant models with $T_{\rm eff}$ around 12,000 K have rather stabilizing outer layers (with Γ_1 slightly above 4/3; see Fig. 4) because the partial photoionization region where $\bar{x} \simeq 0.5$ occurs deeper.

We note, however, that we have set the radiation temperature equal to $T_{\rm eff}$ and $W = \frac{1}{2}$ or $(3 - \sqrt{5})/6$ in our calculations. More accurate computations of the detailed NLTE ionization balance, in which $T_{\rm rad}$ varies with height over the atmosphere and radiation pressure also dilutes with distance, are required to determine the precise boundary parameters at which the models become dynamically unstable in the H-R diagram. Such calculations require "case studies" of various individual supergiants. These stars can have very fast winds and high mass-loss rates, which strongly influence the atmospheric extension. Likewise, we expect that small deviations from an "average" radiation temperature (but which is proportional to $T_{\rm eff}$) will occur because of variations in the local opacity sources at different atmospheric levels. This $T_{\rm rad}$ dependency should

be obtained from accurate observations of their spectral energy distributions.

Our present calculations, which omit these further refinements, show, however, a clear trend in which $\langle\Gamma_1\rangle$ assumes minimum values below 4/3 in stable models of supergiants with $6500 \leq T_{\rm eff} \leq 7500$ K. These atmospheres exist in the extension of the Cepheid instability strip, which has well-defined borders in the H-R diagram. In this area, the smallest values for $\langle\Gamma_1\rangle$ occur down to the base of these atmospheres, practically independent of the gravity acceleration. This indicates the possible relation between pulsation variability and dynamic destabilization mechanisms, caused by the decrease of $\langle\Gamma_1\rangle$. Soukup & Cox (1996) found with time-dependent calculations that the atmospheres of these massive stars become unstable to radial pulsations. They also mention that helium ionization dominates as the driving mechanism, and the contribution from the (thermal) hydrogen ionization zone becomes significant below 5000 K. Long-term spectroscopic and photometric observations of ρ Cas, with $T_{\rm eff} = 6500$–7250 K and $\log (L_*/L_\odot) = 5.6$–5.9, demonstrate that nonradial pulsation modes are excited in these extended atmospheres (Lobel et al. 1994). In a theoretical study of oscillations in cool stars with $\log (L_*/L_\odot) = 5$, Shibahashi & Osaki (1981) found that stable nonradial modes with $l = 10$ can be excited by the ionization zones. When the hydrogen and helium ionization zones are situated too shallowly they cannot excite radial pulsations, but they can drive nonradial modes, which are trapped near the stellar surface. For dynamically stable models, pulsation driving occurs in regions where Γ_3 approaches unity. Lobel et al. (1992) demonstrated that for conditions of cool supergiant atmospheres, the decrease of Γ_3 strongly couples with the decrease of Γ_1 in the partial ionization zones. These considerations imply that the minima we compute for Γ_1 and $\langle\Gamma_1\rangle$ for low-gravity stars in the extension of the Cepheid strip can be related to the excitation of stable nonradial pulsations by partial NLTE ionization of hydrogen in the optically thin part of the atmosphere.

Furthermore, Shibahashi & Osaki (1981) mention convectively unstable zones located just below the photosphere due to hydrogen ionization in their model with $T_{\rm eff} = 7080$ K. In the model with $T_{\rm eff} = 8000$ K, the ionization region emerges above the photosphere, which causes a strong difference between the modal properties of the two models. In hydrodynamic simulations of compressible convection, which consider the effects of partial (LTE) ionization of hydrogen, Rast (1992) mentions the importance of coupling convection with pulsations in Cepheids. From an observational point of view, we note that photospheric absorption lines of yellow hypergiants display an unusually large macrobroadening, which cannot be attributed to rapid rotation (i.e., large $v \sin i$ values) for these evolved and very extended stars. For example, line-profile modeling of high-dispersion observations in ρ Cas yield macrobroadening velocities of $\sim$25 km s^{-1} (see Fig. 3 of Lobel et al. 1998). Fast large-scale velocities are possibly linked with ionization-induced formation of supersonic vertical flows (plumes), simulated for cool low-luminosity stars (e.g., Rast & Toomre 1993).

Another remarkable aspect of yellow hypergiants (for a review see de Jager 1998) are "eruptions," which occur on timescales much longer than the pulsation quasi period (about half a century, say). In an outburst of 1945–1946, ρ Cas (F8p) suddenly dimmed and displayed TiO bands in its spectrum, characteristic of the photospheric temperatures of M-type stars. Within a couple of years (1947 April), the star brightened up by nearly a magnitude, and a mid G-type spectrum was recovered around 1950. In 1985–1986 the star showed a larger-than-average amplitude in the light curve, which could be associated with shell ejection events (Zsoldos & Percy 1991). Pulsational driving with the occurrence of strong convective motions may excite unstable modes with very fast growth rates, resulting in episodic mass ejection. If such a mechanism can account for eruptions of yellow hypergiants, we expect that it is substantially different for the eruptions of LBVs, because strong convective motions induced by partial hydrogen ionization are not expected for these stars, and we compute $\langle\Gamma_1\rangle$ values above 4/3 over the entire atmosphere of hydrostatically stable models with $T_{\rm eff} > 16{,}000$ K.

In a series of papers, Nieuwenhuijzen & de Jager (1995), de Jager & Nieuwenhuijzen (1997), and Nieuwenhuijzen & de Jager (2000) presented strong theoretical and observational indications for the existence of a region in the upper H-R diagram where the atmosphere of yellow hypergiants become unstable. The cool boundary of the "yellow evolutionary void" occurs for *blueward*-evolving massive supergiants at $T_{\rm eff} \simeq 8300$ K and $\log (L_*/L_\odot) > 5.6$. Evolutionary calculations show that these stars are expected to evolve along tracks of nearly constant luminosity, below the Humphreys-Davidson limit. They evolve blueward because massive stars shed copious amounts of mass to the circumstellar/interstellar environment in the red supergiant phase. During redward evolution, the very high mass-loss rates reduce the stability of the convective layer, and below a critical envelope mass it contracts into a thinner radiative envelope, which causes rapid blueward evolution. Only for a limited range of initial masses do stars become red supergiants and evolve back far blueward. A possible candidate for such a scenario is HR 8752, for which Israelian, Lobel, & Schmidt (1999) found an increase of the photospheric temperature by 3000–4000 K, based on high-resolution spectra collected over the past 30 years. It is suggested that recurrent eruptions in yellow hypergiants occur when these stars approach the cool boundary of the void, and "bounce off" redward. The bouncing against the void may also explain why most of the cool luminous hypergiants cluster near its low-temperature boundary, while the identification of hypergiants of later spectral type, possibly such as VY CMa (of M type), is seldom.

In their analysis of atmospheric acceleration mechanisms, Nieuwenhuijzen & de Jager (1995) show that stable solutions cannot be computed for the atmospheres of blueward-evolving yellow hypergiants at the low-temperature boundary of the void. This is a consequence of a time-independent solution of the momentum equation, which considers the Newtonian gravity acceleration derived from the evolutionary mass, the gas, radiation, and turbulent pressure gradients, and the momentum of the stellar wind. The latter requires the observed mass-loss rate. An "effective acceleration" for the atmosphere is obtained iteratively, but becomes negative at the cool border of the void. The outward-directed net force causes an unstable atmosphere around $T_{\rm eff} = 8300$ K. We note that their momentum equation incorporates the important compressibility effects due to thermal ionization by the decrease of Γ_1 in the adiabatic sound velocity, and of the isothermal and iso-

choric factors (χ_ρ and χ_T) in the gas-pressure gradient. We suggest that the determination of instability boundaries for the void be further improved with the NLTE calculations of Γ_1 we present. It is important to note that in our computations the minimum of $\langle\Gamma_1\rangle$ for stable models with lowest gravity acceleration occurs around $T_{\rm eff} = 6500$ K, which does not coincide with the low-temperature border of the void. However, there is an overlap because $\langle\Gamma_1\rangle$ approaches values very close to 4/3 in low-gravity models at this border. This suggests that the minima we compute for $\langle\Gamma_1\rangle$ are rather linked with the driving of stable nonradial pulsation modes for the atmospheres of yellow supergiants in the extension of the Cepheid instability strip, whereas the void can result from a particular combination of various acceleration mechanisms, combined with the decrease of the overall stability by the larger atmospheric compressibility due to partial NLTE and LTE ionization. The high mass-loss rates observed for these streaming atmospheres are also determined by the sonic point, which is situated inside the photospheres of cool massive supergiants. The dynamics of such extended atmospheres must therefore be linked with a prominent mechanism that drives these atmospheric pulsations, and that provides the momentum for their supersonic winds.

Finally, we remark that more definitive conclusions about atmospheric variability mechanisms should be obtained with fully time-dependent hydrodynamic simulations for a number of prototypical hypergiants, such as ρ Cas. Our analytical approximations are useful to evaluate important hydrodynamic quantities such as the adiabatic sound speed $v_{\rm ad}^2 = \Gamma_1 P_t/\rho$ in conditions of NLTE, without having to numerically solve for large systems of nonlinear balance equations. With this analytical work we also provide a well-founded basis for more sophisticated numerical hydrodynamic calculations. Time-dependent codes that simulate the pulsation of extended atmospheres (i.e., as described by Bessell, Scholz, & Wood 1996; Sasselov 1993) could be adequately updated for hydrodynamic NLTE effects without the loss of their numerical efficiencies. With the present study we demonstrate that such advanced calculations cannot be based on the usual assumption of local thermodynamic equilibrium. In extended atmospheres, the thermodynamics of nonlocal equilibrium is required, and ultimately, these calculations also ought to consider nonequilibrium thermodynamic processes for realistic dynamic modeling.

9. CONCLUSIONS

1. We present new expressions for the first generalized adiabatic index Γ_1 and the heat capacities that are required for the study of dynamic stability of supergiant stellar atmospheres. Our equations consider important NLTE effects on the local ionization state by an incident and diluted radiation field, not in equilibrium with the local kinetic gas temperature. We demonstrate analytically that our more general expressions, which are also valid for multicomponent gas mixtures, simplify to the classic formulae in which the radiation and kinetic temperature equilibrate.

2. From a numerical application of our formalism to a grid of supergiant model atmospheres with solar abundance and $4000 \leq T_{\rm eff} \leq 20{,}000$ K, we find that the local values of Γ_1 become very small, below 4/3, over a large fraction of the atmosphere for models with $T_{\rm eff}$ between 7000 and 8000 K. This results from the incident radiation field with a temperature of the order of the stellar effective temperature, which primarily causes partial photoionization of hydrogen. These regions displace deeper down the atmosphere with raising $T_{\rm eff}$, whereas the thermal partial ionization regions, at the base of the atmosphere, displace outward. This combined effect causes the deep minimum in the local values of Γ_1 to occur for these cool star atmospheres. Around these effective temperatures, partial NLTE ionization causes very high atmospheric compressibilities, by which Γ_1 can even decrease to below unity.

3. Numerical evaluations of Ledoux' stability integral $\langle\Gamma_1\rangle$ down into the stellar envelope demonstrate that $\langle\Gamma_1\rangle$ exceeds 4/3 in supergiant models for which we can compute a hydrostatically stable solution. Toward smaller gravity accelerations $\langle\Gamma_1\rangle$ decreases, and models become unstable with $\langle\Gamma_1\rangle < 4/3$ at the base of the envelope. Stable models with smaller atmospheric gravity assume smaller $\langle\Gamma_1\rangle$ values, and Ledoux' stability integral verifies that models of higher $T_{\rm eff}$ destabilize at increasingly larger gravity values because of the enhancement of radiation pressure.

4. Most importantly, our calculations reveal that for stable supergiant models with $6500 \leq T_{\rm eff} \leq 7500$ K, $\langle\Gamma_1\rangle$ assumes minimum values, below 4/3, over a very large fraction of the atmosphere down to its base. Around $T_{\rm eff} = 6500$ K this minimum occurs practically independently of the atmospheric gravity acceleration. These effective temperatures should be considered valid only within a case study for Kurucz atmospheric models. For a given $T_{\rm eff}$, in atmospheres of increasingly smaller gravity, $\langle\Gamma_1\rangle$ assumes small values in layers of increasingly lower density because of enhanced partial ionization with the dilution of the radiation field. This corresponds to dynamically destabilizing regions, extending over an increasingly larger geometric fraction in the upper atmospheres of more massive cool supergiants.

I thank C. de Jager at SRON-Utrecht for many discussions about the physics of supergiant atmospheres, which have stimulated the development of this theoretical work over the past two years. R. Kurucz is gratefully acknowledged for calculating the new grid of atmospheric models and helpful discussions. The referee is thanked for several useful comments. This research is supported in part by an STScI grant GO-5409.02-93A to the Smithsonian Astrophysical Observatory.

APPENDIX

The first adiabatic index is defined by the adiabatic thermodynamic derivative,

$$\Gamma_1 \equiv \left(\frac{\partial \ln P_t}{\partial \ln \rho}\right)_{\rm ad}, \tag{A1}$$

which can also be expressed by combining three thermodynamic quantities,

$$\Gamma_1 = \frac{c_{P_t}}{c_v}\,\chi_\rho\,, \tag{A2}$$

where c_v, c_{P_t}, and χ_ρ denote the heat capacity at constant volume and at constant total pressure, and the isothermal factor, respectively. The total pressure, including the radiation pressure, is given by the equation of state,

$$P_t = P_g + P_{\rm rad} = NkT_e(1+\bar{x})\rho + \tfrac{1}{3}aWT_{\rm rad}^4\,, \tag{A3}$$

where k is the Boltzmann constant, N is the total number of particles per unit mass, and a is the radiation density constant. Here W is the geometric dilution function for the radiation pressure with distance d from the stellar surface R_*. At the surface $z = d/R_* = 1$, and hence $W(z=1) = \frac{1}{2}$, with

$$W(z) = \frac{1}{2}\left(1 - \sqrt{1 - \frac{1}{z^2}}\right). \tag{A4}$$

The ionization equation, modified for photoionization from the ground level for every element i, is (§ 2.1)

$$\frac{x_i}{1-x_i}\,\bar{x} = C_i W\,\frac{T_e^{1/2}}{\rho}\,T_{\rm rad}\exp\left(-\frac{I_i}{kT_{\rm rad}}\right), \tag{A5}$$

where C_i is a constant, and x_i the ionization fraction of element i, which is singly ionized from the ground level, with ionization energy I_i, by the incident radiation field of temperature $T_{\rm rad}$. We denote the mean ionization fraction of the mixture with m elements,

$$\bar{x} = \sum_{i=1}^{m} v_i x_i\,, \tag{A6}$$

where $v_i = N_i/N$ is the element abundance having N_i particles per unit mass, and $\sum_i v_i = 1$ or $N = \sum_i N_i$. Hence, the total number of electrons per unit mass is $N_e = \bar{x}N$.

When the radiation temperature $T_{\rm rad}$ and the kinetic gas temperature T_e are independent quantities, the specific heat capacity (per unit mass) at constant volume v (or density, since $v = 1/\rho$) is defined as the sum of the internal energy derivatives to both independent temperatures,

$$c_v \equiv \left(\frac{\partial e}{\partial T_e}\right)_{\rho, T_{\rm rad}} + \left(\frac{\partial e}{\partial T_{\rm rad}}\right)_{\rho, T_e}. \tag{A7}$$

The internal energy function in equation (A7) is given by

$$e = NkT_e\left[\frac{3}{2}(1+\bar{x}) + \sum_{i=1}^{m} v_i\left(x_i\,\frac{I_i}{kT_e} + x_i\,\frac{w_i}{u_i} + x_i^0\,\frac{w_i^0}{u_i^0}\right)\right] + \frac{aWT_{\rm rad}^4}{\rho}\,, \tag{A8}$$

where $x_i^0 = 1 - x_i$ denotes the neutral particle fraction. The two electronic energy terms of equation (A8) include the partition functions, which are defined by $u_i = \sum_{r=0}^{\infty} g_{r,i}\exp(-\chi_{r,i}/kT_e)$ and $w_i = \sum_{r=0}^{\infty} g_{r,i}(\chi_{r,i}/kT_e)\exp(-\chi_{r,i}/kT_e)$, where $g_{r,i}$ is the statistical weight of the rth excitation level. The partition functions of the neutral fractions are indicated with the zero (0) superscript.

In conditions of stellar atmospheres, the kinetic and ionic terms largely outweigh the electronic terms, and since we assume ionization from the ground level only, the electronic terms can be neglected, yielding

$$e = \frac{3}{2}\,NkT_e(1+\bar{x}) + N\sum_{i=1}^{m} v_i x_i I_i + \frac{aWT_{\rm rad}^4}{\rho}\,. \tag{A9}$$

The specific heat capacity at constant total pressure in equation (2) is defined as the sum of the derivatives of the enthalpy function $h = e + P_t/\rho$ to both independent temperatures,

$$c_{P_t} \equiv \left(\frac{\partial h}{\partial T_e}\right)_{P_t, T_{\rm rad}} + \left(\frac{\partial h}{\partial T_{\rm rad}}\right)_{P_t, T_e}, \tag{A10}$$

where

$$h = \frac{5}{2} NkT_e(1 + \bar{x}) + N \sum_{i=1}^{m} v_i x_i I_i + \frac{(4/3)aWT_{\rm rad}^4}{\rho} . \tag{A11}$$

We proceed by deriving the detailed expressions for the individual terms of equations (A7) and (A10).

In equation (A7) the kinetic temperature derivative at constant density yields

$$\left(\frac{\partial e}{\partial T_e}\right)_\rho = \frac{3}{2} Nk\left[(1 + \bar{x}) + T_e\left(\frac{\partial \bar{x}}{\partial T_e}\right)_\rho\right] + N \sum_i v_i I_i \left(\frac{\partial x_i}{\partial T_e}\right)_\rho , \tag{A12}$$

and the radiation temperature derivative yields

$$\left(\frac{\partial e}{\partial T_{\rm rad}}\right)_\rho = \frac{3}{2} NkT_e\left(\frac{\partial \bar{x}}{\partial T_{\rm rad}}\right)_\rho + N \sum_i v_i I_i \left(\frac{\partial x_i}{\partial T_{\rm rad}}\right)_\rho + 12\alpha\theta Nk(1 + \bar{x}) , \tag{A13}$$

where α is the ratio of the radiation pressure and the kinetic gas pressure, $P_{\rm rad}/P$, and θ is the ratio of the local kinetic temperature and the temperature of the incident radiation field, $T_e/T_{\rm rad}$.

In equation (A10) the kinetic temperature derivative at constant total pressure yields

$$\left(\frac{\partial h}{\partial T_e}\right)_{P_t} = \frac{5}{2} Nk\left[(1 + \bar{x}) + T_e\left(\frac{\partial \bar{x}}{\partial T_e}\right)_{P_t}\right] + N \sum_i v_i I_i \left(\frac{\partial x_i}{\partial T_e}\right)_{P_t} - 4\alpha Nk(1 + \bar{x})\left(\frac{\partial \ln \rho}{\partial \ln T_e}\right)_{P_t} , \tag{A14}$$

and the radiation temperature derivative casts by using $P_{\rm rad} = \frac{1}{3} aWT_{\rm rad}^4$ into

$$\left(\frac{\partial h}{\partial T_{\rm rad}}\right)_{P_t} = \frac{5}{2} NkT_e\left(\frac{\partial \bar{x}}{\partial T_{\rm rad}}\right)_{P_t} + N \sum_i v_i I_i \left(\frac{\partial x_i}{\partial T_{\rm rad}}\right)_{P_t} + 4\alpha Nk\theta(1 + \bar{x})\left[4 - \left(\frac{\partial \ln \rho}{\partial \ln T_{\rm rad}}\right)_{P_t}\right] . \tag{A15}$$

Hence, both heat capacities are obtained from the detailed evaluation of two thermodynamic quantities in equations (A12) and (A13):

$$\left(\frac{\partial x_i}{\partial T_e}\right)_\rho \quad \text{and} \quad \left(\frac{\partial x_i}{\partial T_{\rm rad}}\right)_\rho , \tag{A16}$$

and with equation (A6),

$$\left(\frac{\partial \bar{x}}{\partial T_e}\right)_\rho = \sum_i v_i \left(\frac{\partial x_i}{\partial T_e}\right)_\rho \quad \text{and} \quad \left(\frac{\partial \bar{x}}{\partial T_{\rm rad}}\right)_\rho = \sum_i v_i \left(\frac{\partial x_i}{\partial T_{\rm rad}}\right)_\rho . \tag{A17}$$

Four thermodynamic quantities are to be evaluated in equations (A14) and (A15):

$$\left(\frac{\partial x_i}{\partial T_e}\right)_{P_t}, \quad \left(\frac{\partial x_i}{\partial T_{\rm rad}}\right)_{P_t}, \quad \left(\frac{\partial \rho}{\partial T_e}\right)_{P_t}, \quad \text{and} \quad \left(\frac{\partial \rho}{\partial T_{\rm rad}}\right)_{P_t} , \tag{A18}$$

for which also

$$\left(\frac{\partial \bar{x}}{\partial T_e}\right)_{P_t} = \sum_i v_i \left(\frac{\partial x_i}{\partial T_e}\right)_{P_t} \quad \text{and} \quad \left(\frac{\partial \bar{x}}{\partial T_{\rm rad}}\right)_{P_t} = \sum_i v_i \left(\frac{\partial x_i}{\partial T_{\rm rad}}\right)_{P_t} . \tag{A19}$$

1. The kinetic temperature derivative of the ionization equation (A5) at constant density and radiation temperature yields, after grouping terms and some rearrangement,

$$\left(\frac{\partial x_i}{\partial \ln T_e}\right)_\rho = x_i(1 - x_i)\left[\frac{1}{2} - \left(\frac{\partial \ln \bar{x}}{\partial \ln T_e}\right)_\rho\right] , \tag{A20}$$

which casts with equation (A17) (multiplying both sides with $\sum_i v_i$), after factorization, into

$$\left(\frac{\partial \bar{x}}{\partial T_e}\right)_\rho = \frac{1}{2T_e} \frac{\bar{x} \sum_i v_i x_i(1 - x_i)}{\sum_i v_i x_i(1 - x_i) + \bar{x}} . \tag{A21}$$

We obtain by inserting equation (A21) in equation (A20) for every element i,

$$\left(\frac{\partial x_i}{\partial T_e}\right)_\rho = \frac{1}{2T_e} \frac{x_i(1 - x_i) \sum_i v_i x_i}{\sum_i v_i x_i(1 - x_i) + \sum_i v_i x_i} . \tag{A22}$$

Equation (A12) reduces, after inserting equations (A21) and (A22) and grouping terms, to

$$\left(\frac{\partial e}{\partial T_e}\right)_\rho = Nk\left\{\frac{3}{2}(1 + \bar{x}) + \frac{1}{2}\left[\frac{3}{2}\bar{x} - \sum_i v_i x_i(1 - x_i)\frac{I_i}{kT_e}\right] \frac{\sum_i v_i x_i(1 - x_i)}{\bar{x} + \sum_i v_i x_i(1 - x_i)}\right\} + Nk \frac{1}{2} \sum_i v_i x_i(1 - x_i) \frac{I_i}{kT_e} \tag{A23}$$

$$= Nk\left[\frac{3}{2}(1 + \bar{x}) + \frac{\bar{x}}{2} \frac{\sum_i v_i x_i(1 - x_i)(3/2 + I_i/kT_e)}{\bar{x} + \sum_i v_i x_i(1 - x_i)}\right] . \tag{A24}$$

2. Analogously, the radiation temperature derivative of the ionization equation (A5) at constant density and kinetic temperature yields, after grouping terms and some rearrangement,

$$\left(\frac{\partial x_i}{\partial \ln T_{\rm rad}}\right)_\rho = x_i(1-x_i)\left[\left(1+\frac{I_i}{kT_{\rm rad}}\right)-\left(\frac{\partial \ln \bar{x}}{\partial \ln T_{\rm rad}}\right)_\rho\right], \tag{A25}$$

which casts with equation (A17), after factorization, into

$$\left(\frac{\partial \bar{x}}{\partial T_{\rm rad}}\right)_\rho = \frac{1}{T_{\rm rad}}\,\frac{\bar{x}\sum_i \nu_i x_i(1-x_i)(1+I_i/kT_{\rm rad})}{\sum_i \nu_i x_i(1-x_i)+\bar{x}}\,. \tag{A26}$$

We obtain by inserting equation (A26) in equation (A25) for every element i,

$$\left(\frac{\partial x_i}{\partial T_{\rm rad}}\right)_\rho = \frac{1}{T_{\rm rad}}\,x_i(1-x_i)\left[\left(1+\frac{I_i}{kT_{\rm rad}}\right)-\frac{\sum_i \nu_i x_i(1-x_i)(1+I_i/kT_{\rm rad})}{\sum_i \nu_i x_i(1-x_i)+\sum_i \nu_i x_i}\right]. \tag{A27}$$

Equation (A13) reduces, after inserting equations (A26) and (A27) and grouping terms, to

$$\begin{aligned}\left(\frac{\partial e}{\partial T_{\rm rad}}\right)_\rho = {} & Nk\left\{\left[\frac{3}{2}\,\theta\bar{x}-\sum_i \nu_i x_i(1-x_i)\,\frac{I_i}{kT_{\rm rad}}\right]\frac{\sum_i \nu_i x_i(1-x_i)(1+I_i/kT_{\rm rad})}{\bar{x}+\sum_i \nu_i x_i(1-x_i)}\right\}\\ & + Nk\left[\sum_i \nu_i x_i(1-x_i)\,\frac{I_i}{kT_{\rm rad}}\left(1+\frac{I_i}{kT_{\rm rad}}\right)+12\alpha\theta(1+\bar{x})\right].\end{aligned} \tag{A28}$$

Hence, with equation (A7) we obtain the total heat capacity at constant volume by summing equations (A23) and (A28), and grouping terms:

$$\begin{aligned}\frac{c_v}{Nk} = {} & \left(\frac{3}{2}+12\alpha\theta\right)(1+\bar{x})+\sum_i \nu_i x_i(1-x_i)\,\frac{I_i}{kT_e}\left[\frac{1}{2}+\theta\left(1+\frac{I_i}{kT_{\rm rad}}\right)\right]\\ & +\left[\frac{3}{2}\,\bar{x}-\sum_i \nu_i x_i(1-x_i)\,\frac{I_i}{kT_e}\right]\frac{\sum_i \nu_i x_i(1-x_i)[1/2+\theta(1+I_i/kT_{\rm rad})]}{\bar{x}+\sum_i \nu_i x_i(1-x_i)}\,,\end{aligned} \tag{A29}$$

where we normalize the specific heat capacity to the gas constant to obtain dimensionless units. When we denote

$$X = \sum_i \nu_i x_i(1-x_i)\,, \tag{A30}$$

$$Y = \sum_i \nu_i x_i(1-x_i)\,\frac{I_i}{kT_e}\,, \tag{A31}$$

and define the functions Q and G for element i as

$$Q_i = \frac{1}{2}+\theta\left(1+\frac{I_i}{kT_{\rm rad}}\right), \tag{A32}$$

$$G_i = Q_i\left[\frac{(3/2)\bar{x}-Y}{\bar{x}+X}+\frac{I_i}{kT_e}\right], \tag{A33}$$

equation (A29) can formally be expressed as

$$\frac{c_v}{Nk} = \left(\frac{3}{2}+12\alpha\theta\right)(1+\bar{x})+\sum_i \nu_i x_i(1-x_i)G_i\,. \tag{A34}$$

Equations (A30)–(A33) enable a similar compact form for the detailed expression of the heat capacity at constant total pressure, which we obtain below.

3. The kinetic temperature derivative of the ionization equation (A5) at constant total pressure and radiation temperature yields, after grouping terms and some rearrangement,

$$\left(\frac{\partial x_i}{\partial \ln T_e}\right)_{P_t} = x_i(1-x_i)\left[\frac{3}{2}-\frac{1}{\bar{x}(1+\bar{x})}\left(\frac{\partial \bar{x}}{\partial \ln T_e}\right)_{P_t}\right], \tag{A35}$$

which casts with equation (A19), after factorization, into

$$\left(\frac{\partial \bar{x}}{\partial T_e}\right)_{P_t} = \frac{3}{2T_e}\,\frac{\bar{x}(1+\bar{x})\sum_i \nu_i x_i(1-x_i)}{\bar{x}(1+\bar{x})+\sum_i \nu_i x_i(1-x_i)}\,. \tag{A36}$$

We obtain by inserting equation (A36) in equation (A35) for every element i,

$$\left(\frac{\partial x_i}{\partial T_e}\right)_{P_t} = \frac{3}{2T_e}\frac{x_i(1-x_i)\sum_i v_i x_i(1+\sum_i v_i x_i)}{\sum_i v_i x_i(1-x_i)+\sum_i v_i x_i(1+\sum_i v_i x_i)}, \tag{A37}$$

for which we note the formal resemblance to equation (A22), apart from an extra factor $(1 + \sum_i v_i x_i)$ in the numerator and the second term of the denominator.

4. The kinetic temperature derivative of the density at constant total pressure and radiation temperature results from differentiating the equation of state (eq. [A3]),

$$\left(\frac{\partial \ln \rho}{\partial \ln T_e}\right)_{P_t} = -\left[1+\frac{1}{1+\bar{x}}\left(\frac{\partial \bar{x}}{\partial \ln T_e}\right)_{P_t}\right]. \tag{A38}$$

5. The radiation temperature derivative of the ionization equation (A5) at constant total pressure and kinetic temperature yields, after grouping terms and some rearrangement,

$$\left(\frac{\partial x_i}{\partial \ln T_{\rm rad}}\right)_{P_t} = x_i(1-x_i)\left[1+4\alpha+\frac{I_i}{kT_{\rm rad}}-\frac{1}{\bar{x}(1+\bar{x})}\left(\frac{\partial \bar{x}}{\partial \ln T_{\rm rad}}\right)_{P_t}\right], \tag{A39}$$

which casts with equation (A19), after factorization, into

$$\left(\frac{\partial \bar{x}}{\partial T_{\rm rad}}\right)_{P_t} = \frac{1}{T_{\rm rad}}\frac{\bar{x}(1+\bar{x})\sum_i v_i x_i(1-x_i)(1+4\alpha+I_i/kT_{\rm rad})}{\bar{x}(1+\bar{x})+\sum_i v_i x_i(1-x_i)}. \tag{A40}$$

We obtain, by inserting equation (A40) in equation (A29) for every element i,

$$\left(\frac{\partial x_i}{\partial \ln T_{\rm rad}}\right)_{P_t} = x_i(1-x_i)\left[1+4\alpha+\frac{I_i}{kT_{\rm rad}}-\frac{\sum_i v_i x_i(1-x_i)(1+4\alpha+I_i/kT_{\rm rad})}{\sum_i v_i x_i(1-x_i)+\sum_i v_i x_i(1+\sum_i v_i x_i)}\right], \tag{A41}$$

for which we note the formal resemblance to equation (A27), apart from the extra terms with 4α in the numerator, and an extra factor $(1 + \sum_i v_i x_i)$ in the second term of the denominator.

6. The radiation temperature derivative of the density at constant total pressure and kinetic temperature results from differentiating the equation of state (eq. [A3]):

$$\left(\frac{\partial \ln \rho}{\partial \ln T_{\rm rad}}\right)_{P_t} = -\left[4\alpha+\frac{1}{1+\bar{x}}\left(\frac{\partial \bar{x}}{\partial \ln T_{\rm rad}}\right)_{P_t}\right]. \tag{A42}$$

Hence, with equation (A10), we obtain the total heat capacity at constant total pressure by summing equations (A14) and (A15), and grouping terms:

$$\begin{aligned}\frac{c_{P_t}}{Nk} = {} & \left\{\frac{5}{2}+16\alpha\theta-4\alpha\left[\left(\frac{\partial \ln \rho}{\partial \ln T_e}\right)_{P_t}+\theta\left(\frac{\partial \ln \rho}{\partial \ln T_{\rm rad}}\right)_{P_t}\right]\right\}(1+\bar{x}) \\ & +\frac{5}{2}T_e\left[\left(\frac{\partial \bar{x}}{\partial T_e}\right)_{P_t}+\left(\frac{\partial \bar{x}}{\partial T_{\rm rad}}\right)_{P_t}\right]+\sum_i v_i\frac{I_i}{k}\left[\left(\frac{\partial x_i}{\partial T_e}\right)_{P_t}+\left(\frac{\partial x_i}{\partial T_{\rm rad}}\right)_{P_t}\right],\end{aligned} \tag{A43}$$

where we normalize the specific heat capacity to the gas constant to obtain dimensionless units.

When inserting equations (A36)–(A38) and (A40)–(A42) in equation (A43), and defining with equations (A30)–(A32) the function H_i for element i,

$$H_i = (Q_i+1+4\alpha\theta)\left[\frac{(5/2+4\alpha)\bar{x}(1+\bar{x})-Y}{\bar{x}(1+\bar{x})+X}+\frac{I_i}{kT_e}\right], \tag{A44}$$

we obtain, after grouping terms, the formal expression

$$\frac{c_{P_t}}{Nk} = \left\{\frac{5}{2}+4\alpha[4\theta(\alpha+1)+1]\right\}(1+\bar{x})+\sum_i v_i x_i(1-x_i)H_i. \tag{A45}$$

REFERENCES

Anders, E., & Grevesse, N. 1989, Geochim. Cosmochim. Acta, 53, 197
Baschek, B., Holweger, H., & Traving, G. 1966, Abhandl. Hamburger Sternwarte, Band VIII, No. 1 (Hamburg-Bergedorf), 26
Beaudet, G., & Tassoul, M. 1971, A&A, 13, 209
Bessell, M. S., Scholz, M., & Wood, P. R. 1996, A&A, 307, 481
Biermann, L. 1942, Z. Astrophys., 22, 65
Chandrasekhar, S. 1939, Introduction to the Study of Stellar Structure (Chicago: Univ. Chicago Press), 55
Claas, W. J. 1951, Recherches Astron. Obs. Utrecht XII, Part 1
Cox, J. P., & Giuli, R. T. 1968, Principles of Stellar Structure (New York: Gordon & Breach)
Däppen, W., Mihalas, D., Hummer, D. G., & Weibel Mihalas, B. 1988, ApJ, 332, 261
de Jager, C. 1998, A&A Rev., 8, 145
de Jager, C., & Nieuwenhuijzen, H. 1997, MNRAS, 290, L50
Ecker, G. 1978, in Theoretical and Computational Plasma Physics (Vienna: Int. Atomic Energy Agency), 259
Ecker, G., & Kroll, W. 1963, Phys. Fluids, 8, 354
Eddington, A. S. 1918, MNRAS, 79, 2
———. 1919, MNRAS, 79, 177
———. 1926, The Internal Constitution of the Stars (Cambridge: Cambridge Univ. Press), 191
Elliott, J. R., & Kosovichev, A. G. 1998, ApJ, 500, L199
Elwert, G. 1952, Z. Naturforsch. A, 7, 432, 703
Fowler, R. A., & Guggenheim, E. A. 1925, MNRAS, 85, 961
Hartmann, L., & McGregor, K. B. 1980, ApJ, 242, 260

Hummer, D. G., & Mihalas, D. 1988, ApJ, 331, 794
Humphreys, R. M., & Davidson, K. 1994, PASP, 106, 1025
Israelian, G., Lobel, A., & Schmidt M. R. 1999, ApJ, 523, L145
Krishna-Swamy, K. S. 1961, ApJ, 134, 1017
Kurucz, R. L. 1996, in ASP Conf. Ser. 108, Model Atmospheres and Spectrum Synthesis, ed. S. Adelman, F. Kupka, & W. Weiss (San Francisco: ASP), 160
Ledoux, P. 1945, ApJ, 102, 143
———. 1965, Stars and Stellar Systems (Chicago: Univ. Chicago Press)
Lobel, A. 1997, Pulsation and Atmospherical Instability of Luminous F- and G-type Stars (Maastricht: Shaker)
Lobel, A., Achmad, L., de Jager, C., & Nieuwenhuijzen, H. 1992, A&A, 264, 147
Lobel, A., de Jager, C., Nieuwenhuijzen, H., Smolinski, J., & Gesicki, K. 1994, A&A, 291, 226
Lobel, A., Israelian, G., de Jager, C., Musaev, F., Parker, J. W., & Mavrogiorgou, A. 1998, A&A, 330, 659
Maeder, A. 1992, in Instabilities in Evolved Super- and Hypergiants, ed. C. de Jager & H. Nieuwenhuijzen (Amsterdam: North-Holland), 138
Menzel, D. H., Bhatnagar, P. L., & Sen, H. K. 1963, Stellar Interiors (London: Chapman & Hall)
Mihalas, D. 1965, ApJ, 141, 564
Mihalas, D., Däppen, W., & Hummer, D. G. 1988, ApJ, 331, 815
Mihalas, D., Hummer, D. G., Weibel Mihalas, B., & Däppen, W. 1990, ApJ, 350, 300
Mihalas, D., & Weibel Mihalas, B. 1984, Foundations of Radiation Hydrodynamics (Oxford: Oxford Univ. Press)
Möglich, F., Riewe, K. H., & Rompe, R. 1939, Ann. Phys., 35, 735
Mollikutty, O. J., Das, M. K., & Tandon, J. N. 1989, Ap&SS, 155, 249
Nieuwenhuijzen, H., & de Jager, C. 1995, A&A, 302, 811
———. 2000, A&A, 353, 163
Nieuwenhuijzen, H., de Jager, C., Cuntz, M., Lobel, A., & Achmad, A. 1993, A&A, 280, 195
Rast, M. P. 1992, Ph.D. thesis, Univ. Colorado
Rast, M. P., & Toomre, J. 1993, ApJ, 419, 224
Rosa, A., & Unsöld, A. 1948, Z. Astrophys., 25, 20
Rosseland, S. 1936, Theoretical Astrophysics (Oxford: Clarendon)
Sasselov, D. D. 1993, Ap&SS, 210, 329
Shibahashi, H., & Osaki, Y. 1981, PASJ, 33, 427
Siedentopf, H. 1933a, Astron. Nachr., 247, 297
———. 1933b, Astron. Nachr., 249, 53
———. 1935, Astron. Nachr., 255, 157
Soukup, M. S., & Cox A. N. 1996, BAAS, 188, 59.05
Spitzer, L., Jr. 1962, Physics of Fully Ionized Gases (2d Ed.; New York: Wiley Interscience)
———. 1972, Physical Processes in the Interstellar Medium (New York: Wiley)
Stolzmann, W., & Blöcker, T. 2000, A&A, 361, 1152
Stothers, R. B. 1999, MNRAS, 305, 365
Stothers, R. B., & Chin, C.-W. 1994, ApJ, 426, L43
———. 1999, ApJ, 522, 960
Strömgren, B. 1948, ApJ, 108, 242
Unsöld, A. 1938, Physik der Sternatmosphären, mit besonderer Berücksichtigung der Sonne (Berlin: Springer)
———. 1948, Z. Astrophys., 25, 11
———. 1968, Physik der Sternatmosphären, mit besonderer Berücksichtigung der Sonne (Berlin: Springer)
Weymann, R. 1962, ApJ, 136, 844
Woolley, R. v. d. R., & Stibbs, D. W. N. 1953, The Outer Layers of a Star (Oxford: Clarendon)
Zsoldos, E., & Percy, J. R. 1991, A&A, 246, 441